Non-negligible impact of Stokes drift and wave-driven Eulerian currents on simulated surface particle dispersal in the Mediterranean Sea

Siren Rühs[1], Ton van den Bremer[2], Emanuela Clementi[3], Michael C. Denes[1], Aimie Moulin[3], and Erik van Sebille[1]

[1]Institute for Marine and Atmospheric research Utrecht, Utrecht University, 3584 CS Utrecht, The Netherlands

[2]Faculty of Civil Engineering and Geosciences, Delft University of Technology, 2628 CD Delft, The Netherlands

[3]CMCC Foundation - Euro-Mediterranean Center on Climate Change, 73100 Lecce, Italy

Correspondence to: Siren Rühs (s.ruhs@uu.nl)

Abstract. Numerical simulations of marine surface particle dispersal are a crucial tool for addressing many outstanding issues in physical oceanography with societal relevance, such as marine plastic pollution. However, the quality of these Lagrangian simulations depends on the ability of the underlying numerical model to represent the prevailing ocean circulation features. Here, we investigate how simulated marine surface particle dispersal changes, if the – often omitted or only approximated – impact of wind-generated surface waves on the upper ocean circulation is considered. We use velocity fields from a high-resolution coupled ocean-wave model simulation and a complementary stand-alone ocean model simulation for the Mediterranean Sea to answer the following questions: 1) How does the explicit representation of waves impact the simulated surface particle dispersal, and what is the relative impact of Stokes drift and wave-driven Eulerian currents? 2) How accurately can the wave impact be approximated by the commonly applied approach to advect particles with non wave-driven Eulerian currents and Stokes drift from stand-alone ocean and wave models? We find that the representation of surface waves tends to increase the simulated mean Lagrangian surface drift speed in winter through a dominant impact of Stokes drift, and to decrease the mean Lagrangian surface drift speed in summer through a dominant impact by wave-driven Eulerian currents. Furthermore, simulations that approximate the surface wave impact by including the Stokes drift (but ignoring the wave-driven Eulerian currents) do not necessarily yield a better estimate of the surface particle dispersal patterns with explicit representation of the wave impact than simulations that do not include any surface wave impact. Our results imply that – whenever possible – velocity fields from a coupled ocean-wave model should be used for surface particle dispersal simulations.

1 Introduction

30 Understanding how seawater moves around in the global ocean and transports heat, dissolved substances, and particulates, is crucial for solving many outstanding issues in physical oceanography and climate science. Due to limited available observations, seawater pathways are often estimated by making use of the three-dimensional and time-varying oceanic velocity fields computed with numerical models. With so-called Lagrangian ocean analyses methods, large sets of virtual fluid particle trajectories are simulated and statistically evaluated, whereby the quality of the analyses strongly depends on how well the

35 underlying numerical model represents the oceanic velocity fields (van Sebille et al., 2018).

Surface particle dispersal simulations that estimate how floating, i.e., surface-bound, particles are transported by horizontal ocean surface velocities are of particular importance for addressing a range of societally relevant issues, such as marine plastic pollution (van Sebille et al., 2020; Sutherland et al., 2023), oil spills (Spaulding, 2017), larval dispersal and biological connectivity (Christensen et al., 2018; Swearer et al., 2019), as well as search and recovery missions (Breivik et al., 2013).

40 Here, we investigate how the simulated dispersal of surface-bound particles changes, if the – often omitted or only approximated – impact of wind-generated surface waves on upper ocean current dynamics is considered. Under the influence of surface waves, a particle does not only move according to the horizontal Eulerian current velocity $\boldsymbol{u}_E = (u_E, v_E)$ (in the following, unless otherwise noted, velocity vectors represent 2D horizontal velocities), but additionally experiences a net drift in the direction of wave propagation, named Stokes drift $\boldsymbol{u}_S$ (Stokes, 1847; van den Bremer and Breivik, 2018). Moreover, the

45 presence of surface waves alters the Eulerian current field itself, which can then be decomposed into a wave-driven component $\boldsymbol{u}_{Ew}$ and a non-wave-driven component $\boldsymbol{u}_{Enw}$ (e.g., Cunningham et al., 2022). Notably, at least part of the wave-driven Eulerian currents tends to act in the opposing direction of Stokes drift (cf., Higgins et al. (2020) and references therein for a review of this "anti-Stokes" effect). Combining those individual terms, the Lagrangian surface drift velocity of the particle $\boldsymbol{u}_L$ can be expressed as

50 $$\boldsymbol{u}_L = \boldsymbol{u}_{Enw} + \boldsymbol{u}_{Ew} + \boldsymbol{u}_S \qquad (1)$$

The determination of $\boldsymbol{u}_L$ requires a detailed knowledge of the temporally and spatially varying oceanic current and wave fields, as well as their interactions. However, large-scale Lagrangian dispersal simulations nearly always rely on velocity output from ocean models that do not explicitly resolve surface waves, which implies that the wave impact is either not included or only approximated. In particular, an increasing number of Lagrangian studies have used a simple superposition of $\boldsymbol{u}_{Enw}$

55 from an ocean model and $\boldsymbol{u}_S$ from a stand-alone wave model for their Lagrangian trajectory calculations, neglecting $\boldsymbol{u}_{Ew}$ (cf., Tamtare et al. (2022) and references therein). Yet, due to the lack of direct observations and of large-scale coupled ocean-wave models, this approximation is only poorly validated. Specifically, the following questions arise:

(1) How does the representation of surface waves impact the simulated surface particle dispersal? What is the relative impact of the wave-driven Eulerian currents, versus the Stokes drift?

(2) How accurately can the wave impact be approximated by the superposition of non-wave-driven Eulerian currents and Stokes drift obtained from stand-alone ocean and wave models?

We address these questions in a case study for the Mediterranean Sea by comparing Lagrangian surface dispersal simulations with different representations of waves, which were performed with the velocity output of a newly developed realistic high-resolution coupled ocean-wave model configuration and a complementary stand-alone ocean model configuration.

2 Theoretical background and state of the art

2.1 Impact of waves on Lagrangian surface drift velocities

Surface waves can impact Lagrangian surface drift velocities, as expressed by Eq. (1), in two ways: by giving rise to the Stokes drift, and by altering the Eulerian current field itself via wave-driven Eulerian currents (Fig. 1).

The Stokes drift was first described by George G. Stokes, who noted that in the presence of surface waves, a particle experiences a net horizontal drift in the direction of wave propagation (Stokes, 1847). This drift can be explained by (linear) wave kinematics. A particle which oscillates forwards and backwards due to surface waves, travels faster, undergoes a larger displacement, and generally stays longer in the crest phase, where horizontal velocities are directed in direction of wave propagation, compared to the trough phase, where horizontal velocities are directed against the direction of wave propagation (van den Bremer and Breivik, 2018; Guha and Gupta, 2023). As the oscillatory motion related to surface waves decays rapidly with depth, so does the Stokes drift. However, the overall magnitude and vertical shear of the Stokes drift depends on the sea state: under wind-sea conditions, where young, locally generated waves with short wave periods dominate, the magnitude of Stokes drift at the surface is high and it's vertical shear is strong; if long-period swell dominates, Stokes drift is less surface intensified (Breivik and Christensen, 2020; Röhrs et al., 2012).

Wave-driven Eulerian current velocities arise from a combination of different processes related to interactions of the Eulerian currents with the Stokes drift acting on a fluid particle through the so-called Stokes forces (see, e.g., van den Bremer and Breivik (2018) for a review), as well as wave-induced changes in the air-sea momentum and turbulent energy fluxes (see, e.g., Breivik et al. (2015) and Couvelard et al. (2020), and references therein).

The different effects of (nonbreaking) surface waves on the Eulerian mean flow in the form of Stokes forces are described by the wave-averaged momentum equations (e.g., Craik and Leibovich, 1976; Suzuki and Fox-Kemper, 2016). These equations can be represented in different (mathematically equivalent) forms, resulting in different Stokes terms and ultimately different corresponding interpretations of the wave impact. They always include the Stokes-Coriolis force (Hasselmann, 1971, 1970), which – however – appears together either with the vortex force and a wave-induced modification of the pressure (e.g., Craik and Leibovich, 1976) or with the Stokes advection and Stokes shear forces (e.g., Suzuki and Fox-Kemper, 2016). We here focus on the former formulation with the following corresponding interpretation: The Stokes-Coriolis force results from the interactions between Stokes drift and the Coriolis force and modifies the turning of the upper ocean Ekman currents (e.g.,

McWilliams and Restrepo, 1999; Song, 2009; Lewis and Belcher, 2004); the vortex force arises from the interactions between Stokes drift and the mean-flow vorticity and introduces an overturning circulation that explains open-ocean Langmuir cells (Craik and Leibovich, 1976).

The momentum flux from the atmosphere to the ocean is impacted by surface waves in two ways. Firstly, waves modify the
95   sea surface roughness and consequently the regional atmospheric momentum flux (e.g., Charnock, 1955; Li et al., 2020). Secondly, waves alter when, where, and how much of this momentum flux is available to drive ocean currents: As waves grow, they absorb momentum from the wind (also referred to as wave-supported stress), which otherwise would have contributed to driving ocean currents; as waves dissipate, they transfer momentum to ocean currents (also referred to as wave-to-ocean stress) (cf., Breivik et al. 2015, Couvelard et al. 2020). In other words, in the absence of coastlines onto which momentum can be
100   transferred, waves act as a net-zero source and sink of momentum.
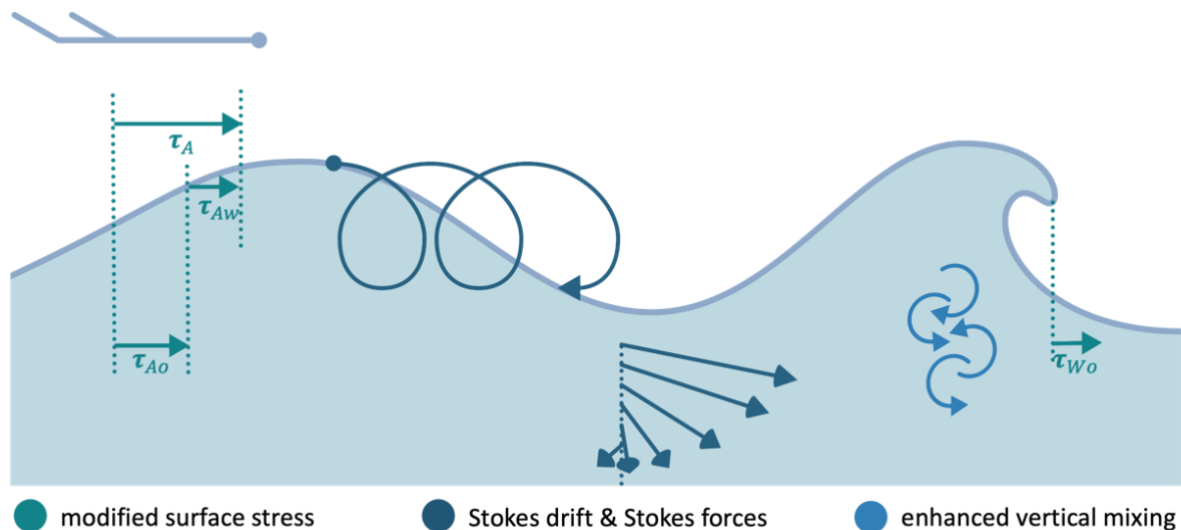
Figure 1: **Sketch of how wind-generated surface waves impact Lagrangian surface drift velocities by giving raise to the Stokes drift and altering the Eulerian current field**. Wave-driven alterations in the Eulerian current field arise from
105   modifications in the surface stress, enhanced vertical mixing, and wave-driven Eulerian currents due to Stokes forces. The Stokes forces include the Stokes-Coriolis force, which alters the upper ocean Ekman currents. Vertical mixing is enhanced, e.g., through wave breaking and Langmuir turbulence. Changes in the surface stress forcing ocean currents (τ_O) result from (i) wave-induced increase in the surface roughness and hence decrease the incoming atmospheric surface stress (τ_A), as well as (ii) growing waves that absorb momentum from the wind (wave-supported stress τ_{Aw}) and dissipating waves that feed
110   momentum back to ocean currents (wave-to-ocean stress τ_{Wo}): $\tau_O = \tau_A - \tau_{Aw} + \tau_{Wo}$. The employed coupled ocean-wave model configuration features a representation of all these impacts, with exception of the regional redistribution of momentum via τ_{Aw} and τ_{Wo} (cf., Sect. 3.1.1). Figure modified after Janssen et al. (2013).

As waves break, they inject turbulent kinetic energy into the surface layer and vertical mixing is enhanced over a depth of the order of the significant wave height (Drennan et al., 1992; Craig and Banner, 1994). Moreover, the wave-averaged flow generates Langmuir turbulence, resulting in vertical mixing over even greater depths (Craig and Banner, 1994) and significantly deepens the mixed layer in large areas of the world ocean (Couvelard et al., 2020). The related hydrographic changes can in turn introduce changes in the horizontal Eulerian currents. These changes in the horizontal Eulerian surface currents due to wave-induced mixing could be as important as the impact of Stokes drift (Rascle et al., 2006; Rascle and Ardhuin, 2009).

2.2 Representation of wave impact in large-scale Lagrangian simulations

So far, in the absence of large-scale operational coupled ocean-wave models, three main approaches have been used to deal with the potential impact of waves on surface particle dispersal simulations, to which we refer to as the "old standard", the "basic approximation", and the "advanced approximation".

If following the old standard, no approximation for the wave impact is applied. Particles are advected solely with $\boldsymbol{u}_{Enw}$ from a stand-alone ocean model. The underlying (implicit) assumption is that impacts of wave-driven Eulerian currents and Stokes drift are either completely negligible or offset one another. For early large-scale dispersal studies, adopting this approach was most likely a pragmatic choice, since the impact of waves has been difficult to measure and to model due to the complex processes that couple the fast and small-scale wave dynamics to the slower and larger-scale motion of ocean currents (cf., Suzuki and Fox-Kemper, 2016).

For the basic approximation, the wave impact is included via a Stokes drift term. Particles are advected with $\boldsymbol{u}_{Enw} + \boldsymbol{u}_S$ from independently run ocean and wave models (or with $\boldsymbol{u}_{Enw}$ and a parameterization of Stokes drift based on the wind speed, cf., Tamtare et al., 2022). Here, the (implicit) assumption is that – at the ocean surface – the impact of wave-driven Eulerian currents is negligible or at least less important than Stokes drift (cf., Clarke and van Gorder, 2018). This approach has been extensively used in a wide range of Lagrangian applications (cf., Tamtare et al., 2022, and references therein). Several studies have attempted a validation of this approach by comparing simulated to observed surface drifter trajectories. While in some studies the inclusion of Stokes drift led to a better agreement between observed and simulated surface drifter trajectories (e.g., Tamtare et al., 2022), others remained inconclusive (e.g., van Sebille et al., 2021). Moreover, Wagner et al. (2022) recently advocated that transport studies that make use of ocean models which do not resolve surface waves should not include a Stokes drift term to estimate the Lagrangian surface drift velocity. Based on a scaling analysis of the wave-averaged momentum equations, they conclude that such wave-agnostic models are not simulating the Eulerian-mean velocity but rather provide fields that are representative for the Lagrangian-mean velocity. This suggests the old standard may indeed be the most appropriate approach for surface particle dispersal simulations.

For the advanced approximation, recently proposed by Higgins et al. (2020), the wave impact is represented via the Stokes
145   drift and an approximation of the wave-driven Eulerian currents. Following this approach, particles are advected with $\boldsymbol{u}_{Enw}$
from a stand-alone ocean model, $\boldsymbol{u}_S$ from a stand-alone wave model, and an offline computed wave-driven Eulerian current
arising largely from the Stokes-Coriolis force. This approach assumes that the impacts of wave-driven Eulerian currents and
Stokes drift are not negligible and do not offset one another, as already suggested by, e.g., Röhrs et al. (2012). Applying the
advanced instead of the basic approximation has been shown to improve the agreement between simulated and observed global
150   marine plastic distributions (Cunningham et al., 2022).

3. Material and Methods

To answer the research questions formulated in Sect. 1 and help solve the long-standing controversy around which of the
approaches introduced in Sect. 2.2 is best suited for surface particle dispersal simulations, we performed and compared
different types of surface particle dispersal simulations based on velocity output from hindcast experiments with a high-
155   resolution coupled ocean-wave model and a complementary non-coupled stand-alone ocean model configurations. The
employed model configurations and corresponding experiments are introduced in Sect. 3.1, and the different types of
Lagrangian surface particle dispersal simulations are described in Sect. 3.2.

3.1 Hindcast experiments with a high-resolution coupled ocean-wave model and a complementary stand-alone ocean model

160   We used the output from a regional high-resolution (ca 4 km horizontal grid spacing) coupled ocean-wave model configuration
and a complementary stand-alone ocean model configuration for the Mediterranean Sea. The coupled configuration is based
on the Mediterranean Sea Physical Analysis and Forecast system developed in the framework of Copernicus Marine Service
(MedFS, version EAS6; Clementi et al., 2021), which was re-run for the IMMERSE H2020 project (https://immerse-ocean.eu/)
with updated model code including advanced representations of wave-current interactions but without data assimilation and
165   without tides in hindcast mode. The Nucleus for European Modelling of the Ocean (NEMO, version 4.2; Madec and the NEMO
System team, 2022) served as the ocean component and the third-generation spectral wave model WaveWatch-III (WW3,
version 6.07; The WAVEWATCH III Development Group, 2019) provided the wave component. The ocean and wave model
components were coupled with the OASIS Model Coupling Toolkit (OASIS3-MCT, version 4.0; Craig et al., 2017). The stand-
alone ocean model configuration is identical to the ocean component of the coupled ocean-wave model configuration, despite
170   for adjustments due to the wave coupling. Hindcast simulations were forced using atmospheric fields from the high-resolution
European Centre for Medium-Range Weather Forecasts (ECMWF HRES). A detailed description and validation of the model
simulations can be found in Moulin and Clementi (2024), we below highlight the aspects most relevant for this study.

3.1.1 The NEMO ocean model

For the coupled and stand-alone regional model configurations, the NEMO hydrodynamic model code is implemented on a
horizontal Arakawa C-grid with 1/24° resolution with 141 unevenly distributed, time-varying vertical levels (z* coordinates).
Bottom cells are partially filled to better represent the model topography. Recent updates in the NEMO code allow for an
improved representation of the impact of waves via modifications in the surface stress driving the ocean currents, the inclusion
of Stokes drift terms in the horizontal momentum, continuity, and tracer advection equations, as well as altered
parameterizations of the sub-grid scale physics (Couvelard et al., 2020). The employed coupled model configuration makes
use of nearly all features described in Couvelard et al. (2020) but uses an alternative formulation for the wave-induced
modification of the surface stress, as summarized below.

In the stand-alone model configuration, the surface wind stress forcing the ocean model $\boldsymbol{\tau}_o$ is calculated via the MedFS bulk
formulae, using relative winds (the difference between the atmospheric winds at 10 m $\boldsymbol{u}_{A10}$ and the oceanic surface current
velocities $\boldsymbol{u}_E(0)$), and a parameterization for the drag coefficient c_d following the formulation of Hellerman and Rosenstein
(1983):

$$\boldsymbol{\tau}_o = \rho_A c_d \|\boldsymbol{u}_{A10} - \boldsymbol{u}_E(0)\|(\boldsymbol{u}_{A10} - \boldsymbol{u}_E(0)), \tag{2}$$

with ρ_A being the atmospheric density.

For the coupled model configuration, the surface wind stress calculation is adjusted to account for wave processes as detailed
in Clementi et al. (2017): by making use of the neutral coefficient from the wave model, the drag coefficient is computed
according to the stable/unstable conditions of the air-sea interface following Large and Yeager (2004). The wave-supported
stress and wave-to-ocean stress (cf. Sect. 2.1, Fig. 1) are not included. Their current implementation breaks the momentum
conservation and hence is not fully satisfactory (Couvelard et al., 2020).

The discretized vertical profile for the horizontal Stokes drift velocity $\boldsymbol{u}_S(z)$ is calculated based on a Phillips spectrum, which
provides a good representation of the Stokes drift velocity near the surface (Breivik et al., 2016). It is derived from the surface
Stokes drift $\boldsymbol{u}_S(0)$ and Euclidean norm of the total (depth-integrated) Stokes transport $\|\boldsymbol{T}_s\|$ from the wave model:

$$\boldsymbol{u}_S(z) = \boldsymbol{u}_S(0)\left[e^{2k_p z} - \beta\sqrt{-2k_p \pi z}\,\text{erfc}\left(\sqrt{-2k_p z}\,\right)\right], \tag{3}$$

$$k_p = \frac{\|\boldsymbol{u}_S(0)\|}{2\,\|\boldsymbol{T}_s\|}\left[1 - \frac{2\beta}{3}\right], \tag{4}$$

with k_p representing the peak wave number and β=1 (as Phillips spectrum is assumed); $erfc$ is the complementary error
function. Due to the C-grid implementation, the horizontal velocity components of the Stokes drift are evaluated at the grid-
cell interfaces. Divergence of the horizontal Stokes drift velocities induces an additional vertical velocity component w_S, which
can be derived from the continuity equation (see below).

The wave-averaged momentum equations for the temporal evolution of the horizontal Eulerian mean velocity $\boldsymbol{u}_E$ are
formulated in the vector-invariant form and – in addition to the usual non-wave-driven terms in the stand-alone ocean model
configuration – include the wave-induced Stokes-Coriolis force $\boldsymbol{W}_{St-Cor}$, vortex force $\boldsymbol{W}_{VF}$, and pressure $\boldsymbol{W}_{Prs}$. The

205   implementation of the former two makes use of the discretized Stokes drift velocity components and the latter of the depth-uniform wave-induced kinematic pressure, also named Bernoulli head term J, directly provided by the wave model:

$$\boldsymbol{W}_{St-Cor} = (fv_S \,, -fu_S), \tag{5}$$

$$\boldsymbol{W}_{VF} = (\zeta v_S - w_s \frac{\partial u}{\partial z} \,, \ -\zeta u_S - w_s \frac{\partial v}{\partial z}), \tag{6}$$

$$\boldsymbol{W}_{Prs} = -\frac{1}{\rho_0}(\frac{\partial J}{\partial x} \,, \frac{\partial J}{\partial y}), \tag{7}$$

210   with f being the Coriolis parameter, ζ the relative vorticity, and ρ_0 a reference density.

The Stokes drift also enters the continuity and three-dimensional tracer advection equations, which take on the following form:

$$\boldsymbol{\nabla} \cdot (\boldsymbol{u}_E + w_E \boldsymbol{k} + \boldsymbol{u}_S + w_S \boldsymbol{k}) = 0, \tag{8}$$

$$\frac{\partial C}{\partial t} = -\boldsymbol{\nabla} \cdot [C(\boldsymbol{u}_E + w_E \boldsymbol{k} + \boldsymbol{u}_S + w_S \boldsymbol{k})] + D^C + F^C, \tag{9}$$

where $\boldsymbol{u}_E$ and $\boldsymbol{u}_S$ are the horizontal Eulerian current and Stokes drift velocity vectors over the $(\boldsymbol{i}, \boldsymbol{j})$ plane, w_E and w_S are the

215   vertical Eulerian current and Stokes drift components with $\boldsymbol{k}$ as the local upward vector, C is the tracer of interest (i.e., temperature T or salinity S), $\boldsymbol{\nabla}$ is the derivative vector operator over the $(\boldsymbol{i}, \boldsymbol{j}, \boldsymbol{k})$ plane, D^C represents parameterizations of small-scale physics, and F^C represents surface forcing terms (i.e., sources and sinks).

The sub-grid scale physics are altered by modifications in the turbulent kinetic energy (TKE) closure scheme and the Langmuir turbulence parameterization, resulting in enhanced vertical mixing. Specifically, the TKE scheme for the coupled configuration

220   includes the production of TKE via Stokes drift shear and its mixing and dissipation length scales are modified to incorporate changes in surface roughness due to waves as well as wave breaking. The surface TKE source is inferred from a wave to ocean energy flux term and changes in surface roughness are inferred from the significant wave height, both provided by the wave model. The Langmuir turbulence parametrization, already employed in the stand-alone ocean model simulation, is improved by using the surface Stokes drift component aligned with the wind as derived from the wave model instead of an approximation

225   of the Stokes drift based on the surface wind stress.

3.1.2 The WW3 wave model

The spectral wave model WW3 is implemented using the same domain and with the same horizontal discretization as the hydrodynamic model. It uses 24 equally distributed directional bins with 15° resolution and 30 frequency bins ranging from 0.0573 Hz to 1.1 Hz to represent the wave spectral distribution. The western boundary is closed, so swells are not entering

230   from the Atlantic.

WW3 solves the wave-action balance equation that describes the evolution of a 2D ocean wave spectrum in the presence of slowly varying currents, whereby an individual spectral component fulfills the linear wave theory. In the employed coupled ocean-wave model configuration, the WW3 implementation is based on the third-order Ultimate Quickest propagation scheme, including the Garden Sprinkler correction (Tolman, 2002). Wind input and dissipation terms are inferred from the wind-wave

235   interaction semi-empirical source terms (ST4; Ardhuin et al., 2010). The non-linear wave-wave interactions are accounted for

by making use of the Discrete Interaction Approximation (DIA; Hasselmann and Hasselmann, 1985). Furthermore, the model incorporates wave-bottom interactions, depth-induced wave breaking (Battjes and Janssen, 1978), and the reflection of waves at the shoreline.

3.1.3 Coupled and non-coupled hindcast experiments

240 Two hindcast experiments were performed: one with the coupled ocean-wave model configuration (in the following also referred to by superscript c), and one with a complementary non-coupled stand-alone ocean model configuration (superscript nc). Both hindcasts use an identical set-up, except for the wave coupling (see Table 1 for a summary of the major differences between the two experiments). The non-coupled experiment was performed first, covering the 3-year period 2018-2020, from which the first year is considered as spin-up. The coupled experiment was then initialized with the oceanic fields on January

245 1st 2019 from the non-coupled experiment and covers the 2-year period 2019-2020.

Table 1: Important specifications of the employed coupled ocean-wave model and complementary stand-alone ocean model experiments. Listed are changes affecting the ocean model component NEMO, grouped according to which parts of the model code they concern, i.e., modifications of the surface stress, additional Stokes terms in the primitive equations, and

250 changes in the sub-grid scale parameterizations.

Model experiment	Modification of surface stress	Inclusion of Stokes drift in NEMO primitive equations			Changes in representation of sub-grid scale physics, i.e., vertical mixing	
		Stokes-Coriolis	vortex force	wave-induced pressure	modifiied TKE scheme	Langmuir turbulence parameterization
non-coupled	NO	NO	NO	NO	NO	Stokes drift approximated
coupled	YES	YES	YES	YES	YES	Stokes drift from wave model

Both hindcast experiments were atmospherically forced by 6-hourly operational analysis and forecast fields from the ECMWF at 1/10° horizontal resolution. Atmospheric momentum and heat fluxes were computed by bulk formulae using the ECMWF atmospheric fields and the model predicted sea surface temperatures, as described in Pettenuzzo et al. (2010) and Tonani et al.

255 (2015). The water balance was computed as evaporation minus precipitation and runoff. While evaporation was indirectly derived from the latent heat flux, precipitation was directly provided as daily averages by ECMWF, and the runoff of the 39 main rivers entering the Mediterranean Sea was obtained as monthly climatological averages from a combination of several data products, as detailed in Clementi et al. (2021).

For the coupled experiment, a one-way hourly exchange of variables (namely the neutral drag coefficient, the sea surface

260 Stokes drift, the total Stokes drift transport, the wave-induced Bernoulli head pressure, the wave to ocean energy flux term, and the significant wave height) from the wave model to the ocean model was realized with the OASIS3-MCT coupler. The

deviation from the two-way coupling approach described in Couvelard et al. (2020) is justified here, since past studies showed that the impact of ocean current variability on wave dynamics is most important for extreme events (Clementi et al., 2017), which are not in the focus of the present study.

265   For our analyses, we make use of the daily mean output for the 2-year period 2019-2020 from the non-coupled and coupled experiments, specifically of the horizontal surface (approximately 1 m depth) Eulerian current and Stokes drift velocities (Fig. 2 shows these velocities from the coupled experiment).
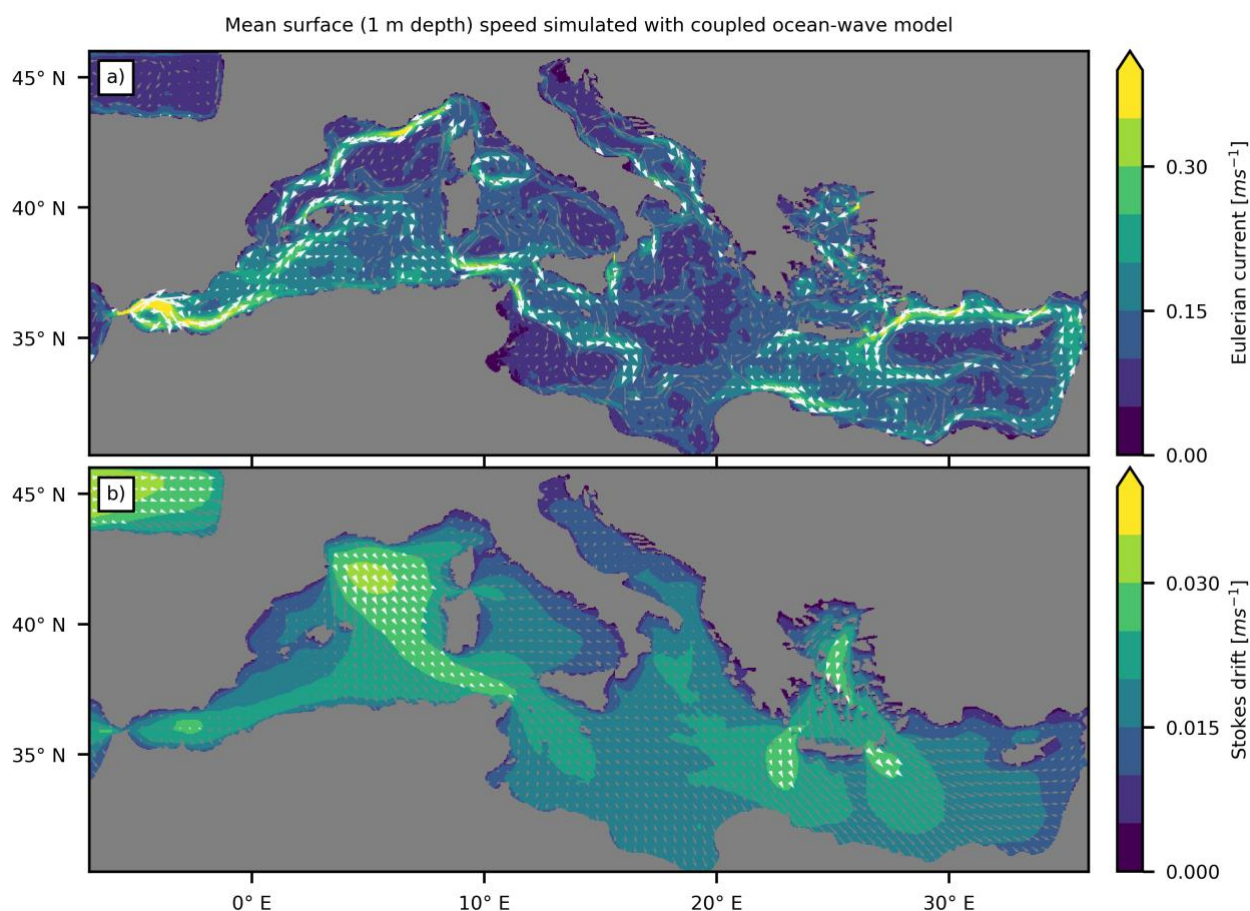
Figure 2: **Lagrangian surface velocity components in the 2-year hindcast with the coupled ocean-wave model**. Mean
270   surface speed (color shading) and direction of mean surface velocities (arrows for every 10th grid point in longitude and latitude direction) in the uppermost ocean grid cell (1 m depth) for **(a)** Eulerian currents (arrows for velocities where mean speed > 0.15 ms^{-1} are rescaled and displayed in white) and **(b)** Stokes drift (arrows for velocities where mean speed > 0.025 ms^{-1} are rescaled and displayed in white).

3.2 Lagrangian surface dispersal simulations

275 We employed the Parcels particle tracking package (version 2.4.0; Lange and van Sebille, 2017; Delandmeter and van Sebille, 2019) to calculate the dispersal of idealized surface-bound Lagrangian particles for different representations of the wave impact. The particles were assumed to be positively buoyant, passive, and dimensionless, so that their movement is completely governed by the horizontal surface velocities. It implies that no vertical motion within the water column, no direct drag with the wind, nor additional behavior patterns were considered. The particles were released uniformly every 0.05° (approximately

280 one particle per model grid cell), every 5 days, over one year (2019), in the uppermost model grid cell (approximately 1 m depth) for three sub-regions in different near-coastal regions of the Mediterranean Sea. The regions were chosen so that they feature different patterns of the impact of waves on Lagrangian surface speed, as detailed in Sect. 4.1: 94243 particles were released in the Gulf of Lion, 98550 in the Gulf of Antalya, and 109427 in the Ionian Sea, east of Sicily. Subsequently, the trajectory calculations were performed using pure horizontal advection forward in time with a 4th order Runge-Kutta scheme

285 and an integration time step of 25 minutes for a total integration time of 30 days. Particle position and speed (time, longitude, latitude, $\|\boldsymbol{u}_L\|$) were stored daily. We did not add any diffusion term, since we aimed at inferring the impact of those processes that are resolved by the coupled versus non-coupled model experiments, and diffusion would add additional noise to this analysis.

We performed 4 complementary types of Lagrangian simulations per release area, all of which follow the general integration

290 scheme outlined above but differ in the surface velocities employed for the particle advection. For each simulation type we made use of a different combination of fields from the non-coupled and coupled ocean model experiments (Table 2). The simulation with only the (non-wave-driven) Eulerian currents from the non-coupled model represents the old standard for Lagrangian simulations not considering any wave effect. The simulation with the (non-wave-driven) Eulerian currents from the non-coupled model and additional Stokes drift from the coupled model is representative for dispersal simulations that

295 employ the basic approximation of the wave effect. It is to note though that the Stokes drift was obtained from the ocean model component on the same grid as the Eulerian currents and not directly from the wave model (see Sect. 3.1.1 for a description of the employed vertical Stokes drift profile). The simulation with (non-wave-driven and wave-driven) Eulerian currents and Stokes drift from the coupled model represents our best guess, with the most realistic representation of the impact of waves on particle dispersal. Additionally, we performed a sensitivity simulation with only the (non-wave-driven and wave-driven)

300 Eulerian currents from the coupled model. This simulation type does not follow any usual approach for surface particle dispersal simulations but is included here to better quantify the impact of waves on surface particle dispersal via Stokes drift versus changes in the Eulerian current velocity. We do not include particle dispersal simulations with the advanced approximation, as this approach is (so far) not widely used and represents an intermediate step between simulations with the basic approximation and our best guess, with presumed limited additional value for answering the research questions outlined

305 in Sect. 1.

Note that, in contrast to what has been reported in various previous studies (e.g., Bosi et al., 2021; Delandmeter and van Sebille, 2019), no significant beaching occurred in any of our Lagrangian simulations. This is related to the fact that all employed velocity fields (Eulerian currents and Stokes drift) were provided on the same ocean model C-grid with zero velocities from ocean to land grid cells, and that these boundary conditions were preserved during the particle tracking with Parcels
310 (Delandmeter and van Sebille, 2019).

Table 2: Performed types of Lagrangian surface dispersal simulations. For each simulation type we employed a different combination of velocity fields from the non-coupled (superscript nc) and coupled (superscript c) model experiments, which represents a different combination of the theoretical non-wave-driven and wave-driven velocity components.

Lagrangian simulation type	Lagrangian velocity components	
	theoretical components	employed modelled velocity fields
old standard	$\boldsymbol{u}_L = \boldsymbol{u}_{Enw}$	$\boldsymbol{u}_L = \boldsymbol{u}_E^{nc}$
basic approximation	$\boldsymbol{u}_L = \boldsymbol{u}_{Enw} + \boldsymbol{u}_S$	$\boldsymbol{u}_L = \boldsymbol{u}_E^{nc} + \boldsymbol{u}_S^c$
best guess	$\boldsymbol{u}_L = \boldsymbol{u}_{Enw} + \boldsymbol{u}_{Ew} + \boldsymbol{u}_S$	$\boldsymbol{u}_L = \boldsymbol{u}_E^c + \boldsymbol{u}_S^c$
sensitivity simulation	$\boldsymbol{u}_L = \boldsymbol{u}_{Enw} + \boldsymbol{u}_{Ew}$	$\boldsymbol{u}_L = \boldsymbol{u}_E^c$

315

4 Results

To obtain a first estimate of the potential impact of the representation of waves on Lagrangian surface dispersal simulations, we evaluate the change in Eulerian averages (that is, grid-based as opposed to particle-based) of the resolved Lagrangian surface drift speed from the coupled simulation compared to the non-coupled simulation (Sect. 4.1). This analysis allows us to
320 define 3 types of regions with distinctively different impact of waves on Lagrangian surface drift speed. We then assess exemplary Lagrangian dispersal simulations for each of these region types and perform a more detailed analysis of the impact of waves on general Lagrangian dispersal statistics such as the along-track distance a particle travels, the magnitude and direction of the net particle displacement, and spatial patterns of particle distributions (Sect. 4.2).

4.1 Impact of waves on Lagrangian surface drift speed

325 Figures 3 and 4 show the change in Eulerian averages of the gridded horizontal Lagrangian surface drift speed from the coupled simulation compared to the non-coupled simulation. The gridded horizontal Lagrangian velocity was defined as $\boldsymbol{u}_L^{nc} = \boldsymbol{u}_E^{nc}$ and $\boldsymbol{u}_L^c = \boldsymbol{u}_E^c + \boldsymbol{u}_S^c$ for the non-coupled and coupled experiment, corresponding to the particle-based Lagrangian velocity definitions of the old standard and the best guess (cf., Table 2), respectively. The total change in the Lagrangian surface drift speed, as well as the Stokes drift and Eulerian current contributions, were then derived as follows: For each model grid point
330 and time step we calculated the surface speed from the zonal and meridional Lagrangian velocity components. In addition, for the coupled simulation, we calculated the scalar projections of the Stokes drift and the Eulerian current velocity onto the total

horizontal Lagrangian velocity vector, which represent the Stokes drift and Eulerian current contributions to the total Lagrangian speed (cf., Appendix A). Subsequently, we derived the total impact of waves and the impact of changes in the Eulerian current component by subtracting the respective values of the non-coupled simulation from the coupled simulation.
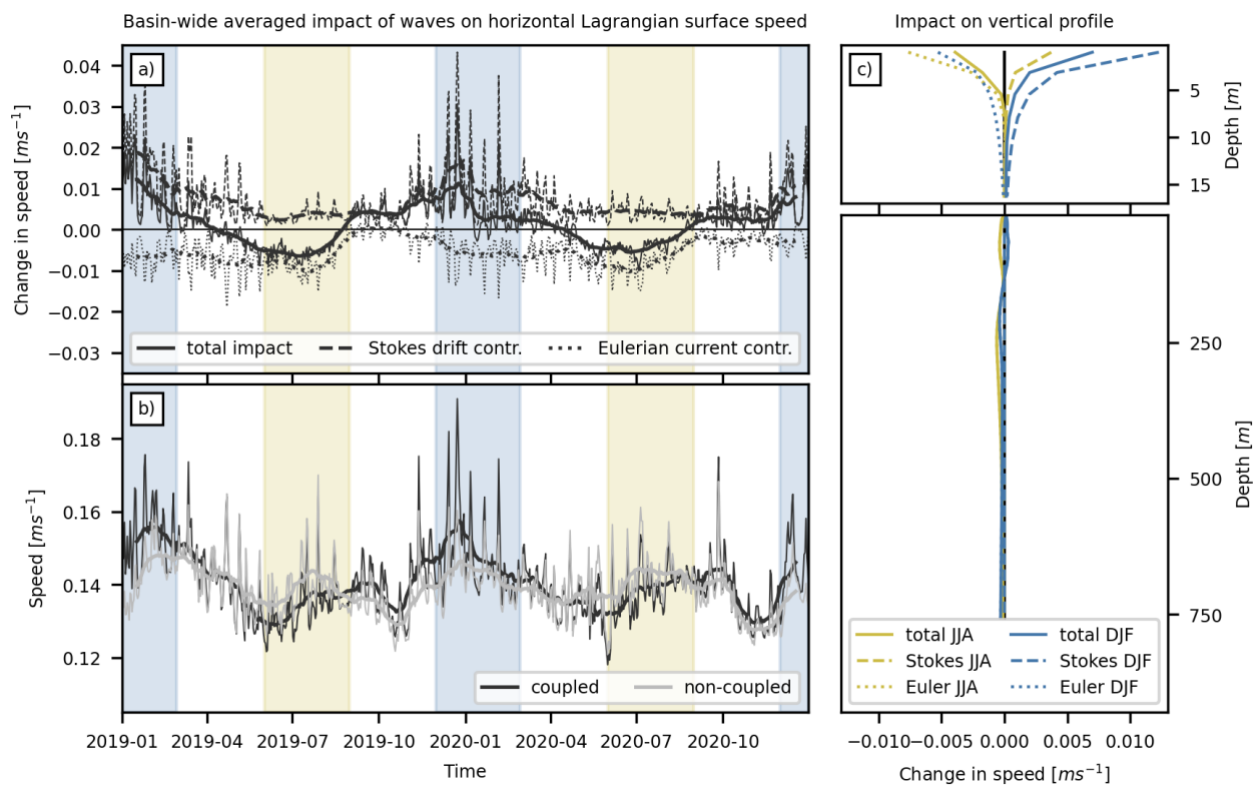
Figure 3: **Impact of surface waves on the simulated horizontal Lagrangian speed averaged over the whole Mediterranean Sea**. **(a)** Temporal variability of the impact of waves on surface speed: daily (thin) and monthly filtered (thick, 30-day running mean) timeseries of the total wave impact (solid line) and the corresponding Stokes drift (dashed line) and Eulerian current (dotted line) contributions. **(b)** Full timeseries of the simulated Lagrangian surface speed for the coupled and non-coupled simulations. **(c)** Vertical profile of the impact of waves for winter (DJF, blue) and summer (JJA, yellow), note that the vertical axis is split and that the Stokes drift component is zero for all depths displayed in the lower part (i.e., the curves for the total impact and the Eulerian current contribution lay on top of each other).

The timeseries of the impact of waves on Lagrangian surface drift speed averaged over the entire Mediterranean Sea reveals distinct and opposing effects of Stokes drift and wave-driven Eulerian currents (Fig. 3a). On the one hand, Stokes drift tends to increase Lagrangian surface speed, in agreement with the general assumptions that wind-generated surface waves predominantly propagate in downwind direction (cf., Clarke and van Gorder, 2018) and that surface currents in the Ekman layer deviate by approximately 45° from the wind direction (cf., Bressan and Constantin, 2019). This increase is – as expected

from the general seasonality of winds and surface wave activity (Barbariol et al., 2021) – weakest in summer and strongest in
350   winter. On the other hand, wave-driven Eulerian currents tend to decrease Lagrangian surface speed, related to the effect of
the anti-Stokes forces and the reduction of atmospheric momentum transfer through increasing surface roughness (cf., Sect.
2.1). This decrease is – somewhat surprisingly – weakest in fall and on average slightly stronger in summer than in winter.

The contrasting seasonality in Stokes drift and wave-driven Eulerian current contributions to Lagrangian surface drift speed
can be largely explained by the related processes acting differently on the vertical velocity profile (Fig. 3c; cf., McWilliams
355   and Restrepo, 1999): while the increase in Lagrangian speed due to Stokes drift is generally occurring only in the upper few
meters in the water column (< 15 m) and features a strong surface-intensification, the decrease in Lagrangian speed due to
wave-driven Eulerian currents reaches much larger depths (> 100 m) and is considerably less surface-intensified in winter than
in summer due to stronger vertical mixing and deeper Ekman layers. If integrated over the whole depth, the wave-driven
decrease of Lagrangian speed due to Eulerian currents is stronger in winter than in summer.

360   The total impact of waves on the Lagrangian surface drift speed appears season-dependent, as the Stokes drift and wave-driven
Eulerian current contributions do not necessarily offset one another (Fig. 3a): in summer, surface drift speed decreases with
wave coupling, dominated by wave-driven Eulerian currents; in winter, surface drift speed increases with wave coupling,
dominated by Stokes drift. As the surface drift speed is generally weaker in summer and stronger in winter, this implies that
the inclusion of waves increases the seasonal variation and hence the temporal variability of simulated Lagrangian surface
365   speed in the Mediterranean Sea (Fig. 3b).

In addition to the seasonal differences, there are regional differences in the total impact of the representation of waves on
Lagrangian surface speed (Fig.4). Here we compare regional averages of the annual, summer (JJA) and winter (DJF) changes
in Lagrangian surface speed for 16 previously defined sub-regions of the Mediterranean Sea that approximately correspond to
its major sub-basins (for a more general description of the dynamics and evaluation of the model performance in these regions
370   see Clementi et al. (2021) and Moulin and Clementi (2024)). Most regions show the previously described pattern of decreased
speed in summer, increased speed in winter, and a small total impact in the annual mean (here termed neutral type regions).
However, there are 4 regions that show increased speed over the whole year, including summer (region numbers 1, 3, 5, and
12; here termed winter type regions), and two regions that show decreased speed over the whole year, including winter (region
numbers 4 and 14; here termed summer type regions). These regional differences are mainly related to differences in the
375   Eulerian current contribution. In contrast to neutral type regions, almost all winter- and summer type regions have stronger
Eulerian current contributions in winter than in summer, with winter values being very negative for the summer type regions
and summer values being only slightly negative or even slightly positive for winter type regions.
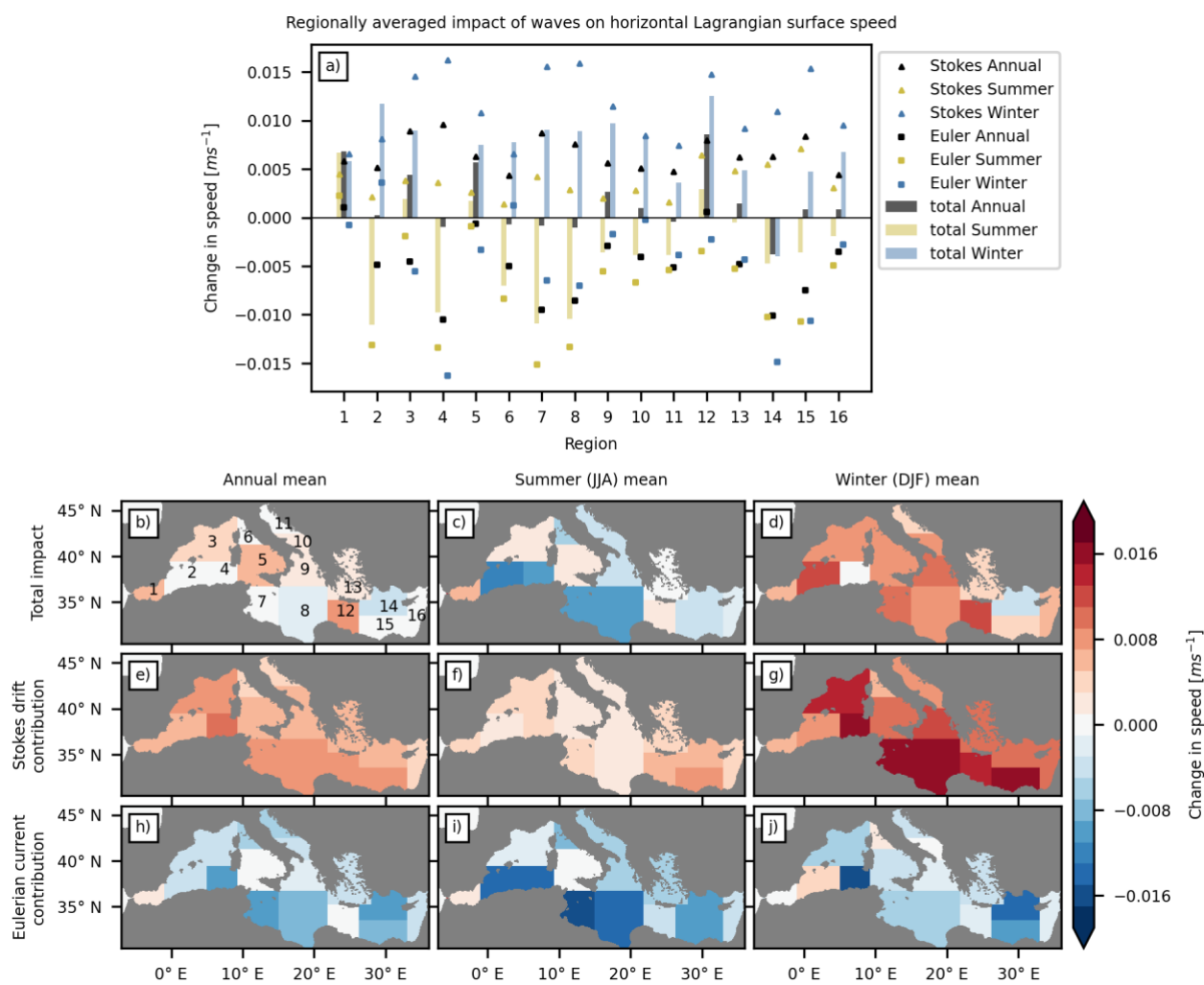
Figure 4: **Regionally averaged impact of the representation of surface waves on simulated mean Lagrangian surface on**
annual, summer, and winter mean speed. Total impact of the representation of waves (bars in (a) and maps (b)-(d)), as well
as the individual contributions of Stokes drift (triangle markes in (a), maps (e)-(g)) and changes in Eulerian currents (square
markers in (a), maps (h)-(j)) are shown. Averages were calculated over the following regions: (1) Alboran Sea, (2) South West
Med 1 (western part), (3) North West Med, (4) South West Med 2 (eastern part), (5) Tyrrhenian Sea 2 (southern part), (6)
Tyrrhenian Sea (northern part), (7) Ionian Sea 1 (western part), (8) Ionian Sea 2 (south-eastern part), (9) Ionian Sea 3 (north-
eastern part), (10) Adriatic Sea 2 (southern part), (11) Adriatic Sea 1 (northern part), (12) Levantine Sea 1 (western part), (13)
Aegean Sea, (14) Levantine Sea 2 (central-northern part), (15) Levantine Sea 3 (central southern part), (16) Levantine Sea 4
(eastern part).

Based on this first analysis of the Lagrangian surface drift speed alone, one could assume that Lagrangian surface dispersal
390 simulations would benefit from using the basic approximation (i.e. adding Stokes drift only) for most regions in winter and for
winter type regions in general, while the old standard may be the preferred choice for most regions in summer and for summer
type regions in general. In the following section, we test this hypothesis by evaluating Lagrangian surface dispersal simulations
with and without (approximated) representation of waves for selected neutral-, winter-, and summer type regions. Figure 5
shows the selected regions together with exemplary simulated trajectories: (1) the neutral type region east of Sicily in the
395 Ionian Sea (2) the Gulf of Lion in the north-west Mediterranean Sea, representing a winter type region, and (3) the Gulf on
Antalya in the central-northern Levantine Sea, representing a summer type region.
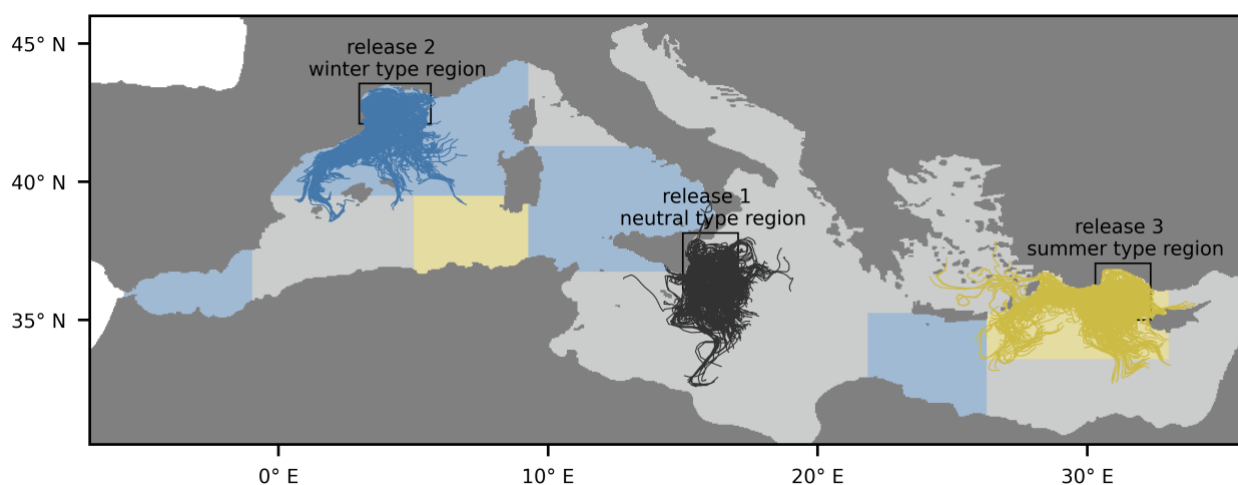
Figure 5: **Exemplary trajectories from the best guess surface particle dispersal simulations**. Trajectories were calculated
for particles released in three areas (indicated by the black frames): the Ionian Sea east of Sicily (release 1, dark grey lines),
400 the Gulf of Lion in the northwest Mediterranean Sea (release 2, blue lines), and the Gulf of Antalya in the central-northern
Levantine Sea (release 3, yellow lines). Background color shading indicates the classification of all previously defined
subregions (cf., Fig. 4) as neutral (light grey), winter (light blue) or summer (light yellow) type.

4.2 Impact of waves on Lagrangian surface dispersal statistics

We assess Lagrangian dispersal statistics in terms of the along-track distance a particle travels, the magnitude and direction of
405 the net particle displacement, as well as spatial patterns of binned particle distributions at the end of the 30-day integration
period. The along-track distance is defined as the length of an individual particle trajectory. The magnitude and direction of
the net displacement are obtained from the vectorial difference between the initial and final position of a particle. Changes in
spatial patterns of binned particle distributions are characterized via changes in the retention rate (the percentage of particles
that remain within or have returned to the region's release area until the end of the integration period), the overall dispersal

410 area (the number of bins occupied with particles), and the area with highest particle concentrations (the bins with the highest number of particle counts that cumultatively encompass 10 % of all particles).

To estimate the total impact of waves on surface dispersal statistics and the individual contributions of Stokes drift and wave-driven Eulerian currents, we compare the four Lagrangian simulation types introduced in Sect. 3.2 (cf., Table 2):

- total wave impact: best guess versus old standard,
415 - Eulerian current impact: sensitivity simulation versus old standard,
- Stokes drift impact: best guess versus sensitivity simulation,
- impact of the basic approximation: basic approximation versus old standard.

It is important to note that the impact of the basic approximation, which results from adding Stokes drift to the Eulerian current fields from the uncoupled model, is distinct from the Stokes drift impact in the best guess simulation. This is due to the fact 420 that for the two different simulation types Stokes drift is combined with different Eulerian velocity fields, so that particles take different trajectories with different along-track values of Stokes drift. To estimate the potential errors that arise from using the basic approximation versus the old standard, we analyze the respective deviations from our best guess experiment.

As in Sect. 4.1, we investigate potential seasonal differences. To do so, summer (JJA) and winter (DJF) trajectories are selected according to their release time. Due to the 30-day integration period for the trajectory calculation, particle positions are partly 425 sampled in September and March for release in summer and winter, respectively.

4.2.1 Ionian Sea east of Sicily (release 1, neutral type region)

In the old standard simulation (Fig. 6a-c, grey bars in Fig. 7, Table 3), particles released east of Sicily predominantly travel south-eastward to south-westward, reaching an average net displacement of 147 km after 30 days, while covering an average along-track distance of 291 km that translates into an average along-track speed of 0.11 ms^{-1}. While individual pathways vary 430 depending on the exact release location and time, and lead to relatively large standard deviations for distance and displacement of 96 km and 80 km, respectively, the distance and displacement distributions clearly show a singular maxima that remain relatively robust throughout the whole year. In winter, there is a slight shift towards shorter distances and smaller but more broadly spatially distributed net displacements compared to summer, the area with the highest particle concentrations is slightly less confined.

435 In the best guess simulation (Fig. 6d-f, black bars in Fig. 7, Table 3), the average along-track distance and net displacement are reduced in summer (-6 % and -13 %, respectively) and enhanced in winter (+10 % and +13 %, respectively) compared to the old standard simulation. The total changes (red lines in Fig. 7) in the distance and displacement distributions are almost completely explained by changes in Eulerian currents (yellow lines in Fig. 7) in summer and by changes due to Stokes drift (blue lines in Fig. 7) in winter. Notably, the changes due to Eulerian currents in summer are of similar magnitude as the changes 440 due to Stokes drift in winter. When considering distance and displacement distributions for the whole year, changes due to Stokes drift and Eulerian currents show opposing tendencies of the same magnitude and result in near zero net changes. These

patterns almost perfectly reflect our finding of Sect. 4.1 for neutral type regions. Moreover, in agreement with decreased Lagrangian speed in summer and increased Lagrangian speed in winter, the retention rate is increased in summer (+19 %) and decreased in winter (-23 %). While the dispersal area remains relatively unchanged in summer (+2 %), it is substantially larger

445 in winter (+20 %).

Whether the basic approximation (Fig. 6g-i, cyan lines in Fig. 7) can improve the simulated wave-driven changes in surface-particle dispersal compared to the old standard is season-dependent (Table 3). Considering only particles released in winter, all calculated dispersion measures show smaller absolute errors when they are inferred from the basic approximation instead of the old standard. Considering all particles or only those particles released in summer, almost all dispersion measures –

450 except for the dispersal area – show better results if the old standard is applied; the absolute error for the basic approximation is, however, in several cases only slightly larger than that for the old standard.
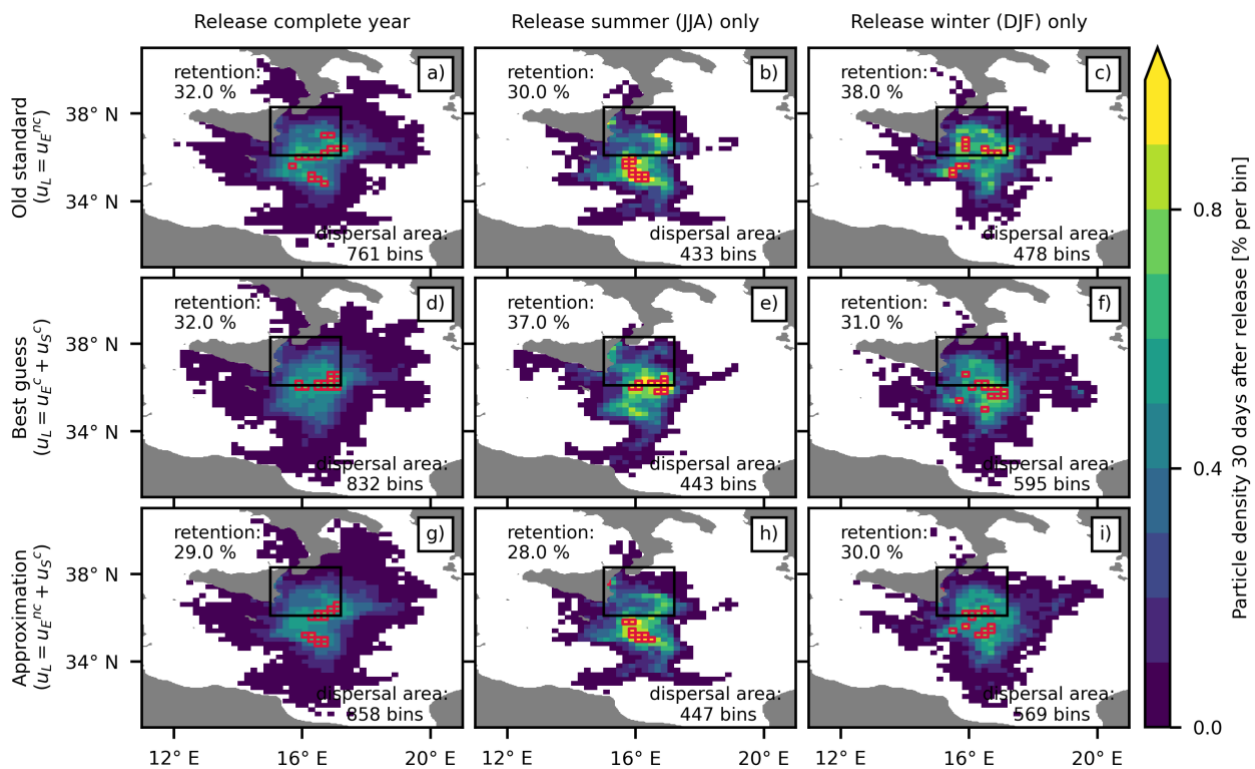
Figure 6: **Impact of surface waves on simulated dispersal pattern of particles released in the Ionian Sea (release 1, neutral type region).** Shown is the particle density per 0.2° x 0.2° bin at the end of the integration period of 30 days (color

455 shading); the area with the highest particle density, encompassing in total 10 % of the particle, is highlighted in red. For better comparability, values of the retention rate (percentage of particles that remain within or have returned to the region's release area, indicated by the black frame, until the end of the integration period) and the overall dispersal area (total number of bins occupied with particles) are printed.
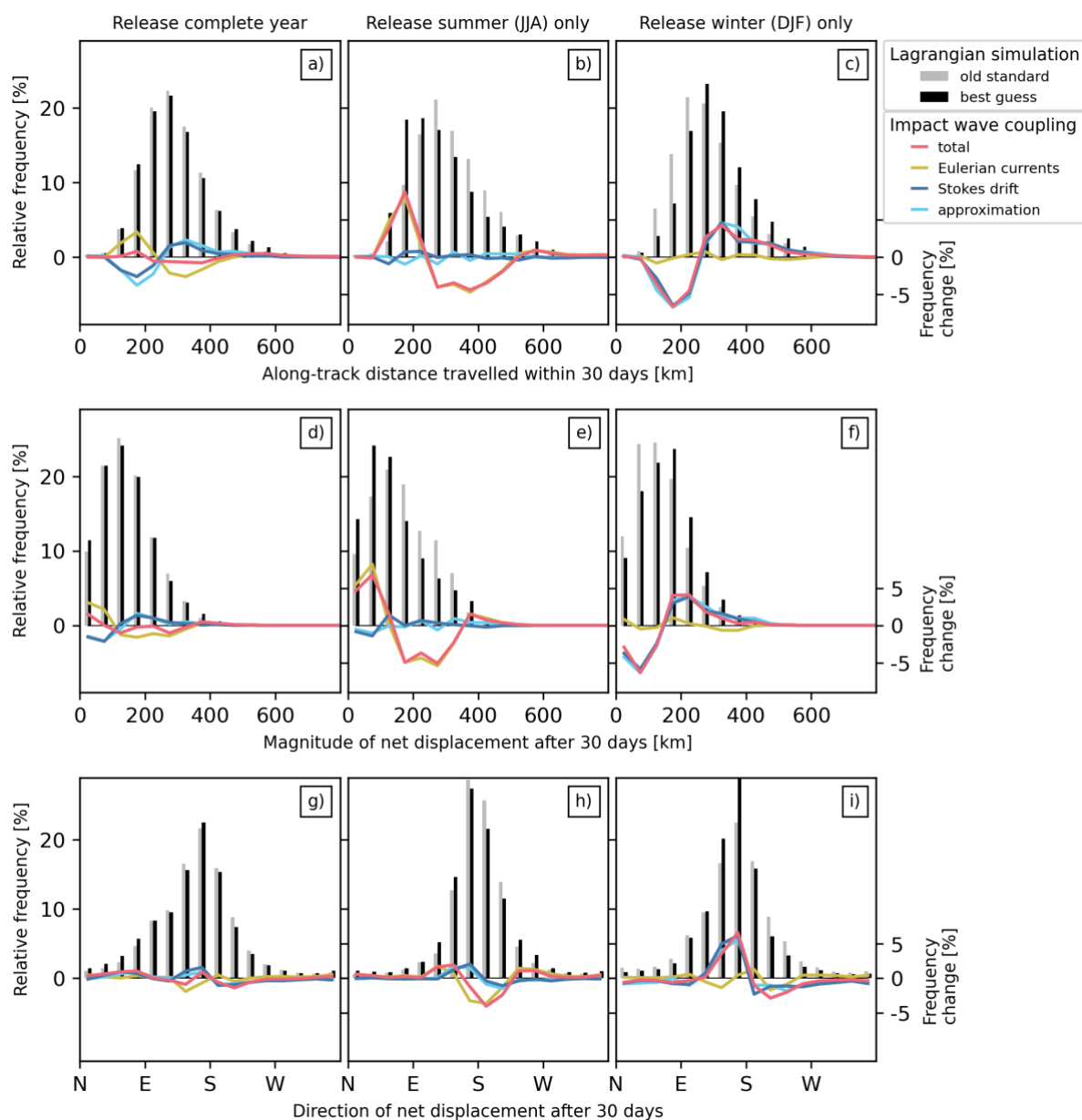
Figure 7: **Impact of surface waves on statistics of simulated dispersal of particles released in the Ionian Sea (release 1, neutral type region) at the end of the integration period of 30 days**. Shown are distributions of (a)-(c) the travelled along-track distance, as well as (d)-(f) the magnitude and (g)-(i) the direction of the net displacement for the old standard (grey bars) and best guess (black bars) simulations; the total change due to the wave coupling (red line), changes resulting from wave-driven Eulerian currents (yellow line) and Stokes drift (blue line) individually, as well as changes resulting from the basic approximation (cyan line) are overlayed.

Table 3: Impact of the representation of surface waves on basic surface particle dispersal measures. The considered measures are the final along-track distance and the magnitude of net displacement (mean +/- standard deviation), as well as the overall retention rate and dispersal area (cf., Sect. 4.2 for their exact definitions). Values are listed for three particle release regions (cf., Fig. 5) and three Lagrangian simulation types (cf., Table 2), together with the absolute errors for simulations 470 performed with the old standard (O) and the basic approximation (A), obtained as the deviation from the best guess (change in percentage in brackets). The last column indicates whether the magnitude of the absolute error is smaller for O or A (differences of 1% or less in brackets). Each cell contains the statistic computed over all released particles (first cell entry), as well as those calculated of subsets of particles released in summer (JJA, second cell entry), and winter (DJF, third cell entry).

Dispersal measure	Release region	Lagrangian simulation type			Absolute error		
		old standard	best guess	basic approx.	error O old standard	error A basic approx.	smaller error
along-track distance [km]	release 1 (neutral type)	291 ± 96	296 ± 108	305 ± 96	-5 (-2%)	+10 (+3%)	(O)
		314 ± 104	297 ± 137	316 ± 106	+16 (+6%)	+19 (+6%)	O/A
		279 ± 100	310 ± 102	315 ± 103	-31 (-10%)	+5 (+1%)	A
	release 2 (winter type)	329 ± 146	345 ± 142	350 ± 138	-16 (-5%)	+5 (+2%)	A
		359 ± 131	357 ± 133	359 ± 122	+1 (+0.3%)	+2 (+0.5%)	(O)
		290 ± 154	332 ± 152	332 ± 152	-42 (-13%)	+1 (+0.3%)	A
	release 3 (summer type)	417 ± 179	407 ± 194	415 ±178	+10 (+2%)	+8 (+2%)	O/A
		407 ± 151	371 ± 152	401 ±145	+35 (+10%)	+29 (+8%)	A
		463 ± 219	470 ± 228	474 ± 216	-6 (-1%)	+4 (+1%)	O/A
magnitude of displacement [km]	release 1 (neutral type)	147 ± 80	146 ± 84	154 ± 82	+0.8(+0.5%)	+8 (+6%)	O
		166 ± 90	147 ± 99	170 ± 93	+18 (+13%)	+23(+16%)	O
		138 ± 78	157 ± 84	164 ± 88	-20 (-13%)	+6(+4%)	A
	release 2 (winter type)	199 ± 138	215 ± 136	209 ± 128	-16 (-8%)	-6 (-3%)	A
		212 ± 126	227 ± 132	219 ± 118	-15 (-7%)	-8 (-4%)	A
		170 ± 139	200 ± 141	194 ± 136	-30 (-15%)	-6 (-3%)	A
	release 3 (summer type)	213 ± 135	214 ± 143	206 ± 133	-1 (-1%)	-8 (-4%)	O
		210 ± 115	191 ± 108	197 ± 110	+19 (+10%)	+6 (+3%)	A
		263 ± 158	264 ± 170	262 ± 160	-1 (-1%)	-2 (-1%)	O/A
dispersal area [bins]	release 1 (neutral type)	761	832	858	-71 (-9%)	+26 (+3%)	A
		433	443	447	-10 (-2%)	+4 (+1%)	(A)
		478	595	569	-117(-20%)	-26 (-4%)	A
	release 2 (winter type)	580	678	729	-98 (-14%)	+51 (+8%)	A
		380	407	424	-27 (-7%)	+17 (+4%)	A
		433	558	583	-125 (-22%)	+25 (+4 %)	A
	release 3 (summer type)	1093	1030	1060	+63 (+6%)	+30 (+3%)	A
		688	672	644	+16 (+2%)	-28 (-4%)	O
		758	694	750	+64 (+9%)	+56 (+8%)	(A)
retention rate [%]	release 1 (neutral type)	32	32	29	0	-3 (-9%)	O
		30	37	28	-7 (-19%)	-9 (-24%)	O
		38	31	30	+7 (+23%)	-1 (-3%)	A
	release 2 (winter type)	27	21	20	+6 (+29%)	-1 (-5%)	A
		20	17	15	+3 (+18%)	-2 (-12%)	A
		38	27	27	+11 (+41%)	0	A
	release 3 (summer type)	23	23	24	0	+4 (+17%)	O
		20	20	24	0	+4 (+20%)	O
		17	22	18	-5 (-23%)	-4 (-18%)	A

Altogether, the results for this region highlight that Stokes drift as well as wave-driven Eulerian currents can have a non-
475 negligible impact on surface particle dispersal and that their relative importance may be season-dependent. Hence, surface
dispersal simulations should at best be performed with output from coupled ocean-wave models. The hypothesis formulated
in Sect. 4.1 is – with few exceptions – valid for this neutral type region: if coupled ocean-wave model output is not available,
the basic approximation should be preferred for winter dispersal simulations, while the old standard remains the slightly better
choice for summer dispersal simulations.

480 *4.2.2 Gulf of Lion in north-west Mediterranean Sea (release 2, winter type region)*

In the old standard simulation (Fig. 8a-c, grey bars in Fig. 9, Table 3), particles released in the Gulf of Lion travel
predominantly south-eastward to south-westward and reach an average net displacement of 199 km, while covering an average
along-track distance of 329 km within the 30-day integration period that translates into an average along-track speed of 0.13
ms^{-1}. However, as in the Ioanian Sea region previously discussed, individual particle pathways vary significantly depending
485 on the exact release location and time, resulting in a relatively wide distribution of along-track distances and net displacements
(standard deviations of 146 km and 138 km, respectively). The final dispersal area extends far beyond the Gulf of Lion into
the Algerian-Balearic Basin, connecting pathways between the Gulf of Lion and the Balearic Islands are well established. Yet,
there exist profound seasonal differences: In summer, south-westward pathways along the French coast are dominating the
final particle distributions, with the largest number of particles found west of Mallorca. In winter, there are more trajectories
490 with shorter along-track distances and net displacements, resulting in smaller mean along-track distance and magnitude of net
displacement, as well as fewer particles reaching the area west of Mallorca and more particles remaining in the release area.
At the same time, the largest individual displacements are higher, yielding connecting pathways to the area south-west of the
Balearic Islands that are not present in summer. Accordingly, the retention rate and dispersal area are both larger in winter
than in summer.

495 In the best guess simulation (Fig. 8d-f, black bars in Fig. 9, Table 3), the average along-track distance and magnitude of net
displacements are increased to 345 km and 215 km, respectively. The retention rate is reduced, and the dispersal area is
increased compared to the old standard simulation. Notably, this holds for the whole year, though the effect is more pronounced
in winter than in summer (41 % vs 18 % reduction in the retention rate and 22 % vs 7 % percent increase in the dispersal area).
This agrees with the finding of Sect. 4.1, that in the Gulf of Lion – a winter type region – the inclusion of wave effects increases
500 the Lagrangian surface drift speed over the whole year due to a dominant impact of Stokes drift that is intensified in winter.
The absolute error in the retention rate and dispersal area (Table 3) is smaller for the basic approximation (Fig. 8g-i) than for
the old standard. This benefit is also visible in the greatly improved estimates for the mean along-track distance (absolute error
reduced from -13 % to +0.3 %) and the magnitude of net displacement (absolute error reduced from -15 % to -3 %) in winter.
Hence, for this winter type region and the selected dispersion measures, applying the basic approximation indeed yields an
505 improvement compared to the old standard simulation in which wave effects are not accounted for. However, while the old

standard overestimates retention rate and tends to underestimate dispersal area, the basic approximation still tends to underestimate the retention rate and overestimates the dispersal area, as partially compensating effects of wave-driven Eulerian currents are not accounted for (Table 3). Depending on the application of interest, the sign of the error may be crucial, so that the old standard could be preferred over the basic approximation, notwithstanding the larger absolute error. Moreover,

510   individual distinct features of the dispersal pattern and statistics in the best guess simulation cannot be reproduced by applying the basic approximation. While the total change (red lines in Fig. 9) in the winter distributions of distance and displacement can be primarily attributed to changes due to Stokes drift (blue lines in Fig. 9), changes in the summer distributions are largely impacted or even dominated by changes in the Eulerian currents (yellow lines in Fig. 9).
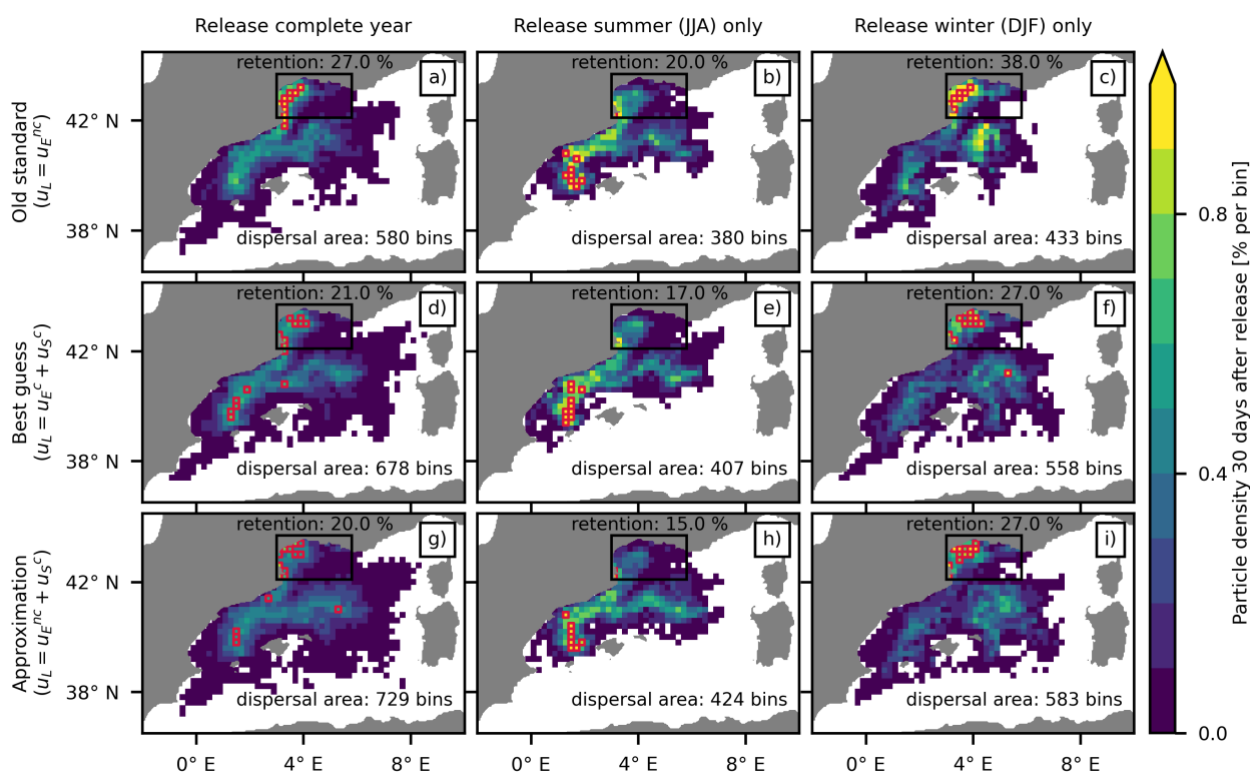
515   **Figure 8**: **Impact of surface waves on simulated dispersal pattern of particles released in the Gulf of Lion (release 2, winter type region)**. Shown is the particle density per 0.2° x 0.2° bin at the end of the integration period of 30 days (color shading); the area with the highest particle density, encompassing in total 10 % of the particle, is highlighted in red. For better comparability, values of the retention rate (percentage of particles that remain within or have returned to the region's release area, indicated by the black frame, until the end of the integration period) and the overall dispersal area (total number of bins

520   occupied with particles) are printed.
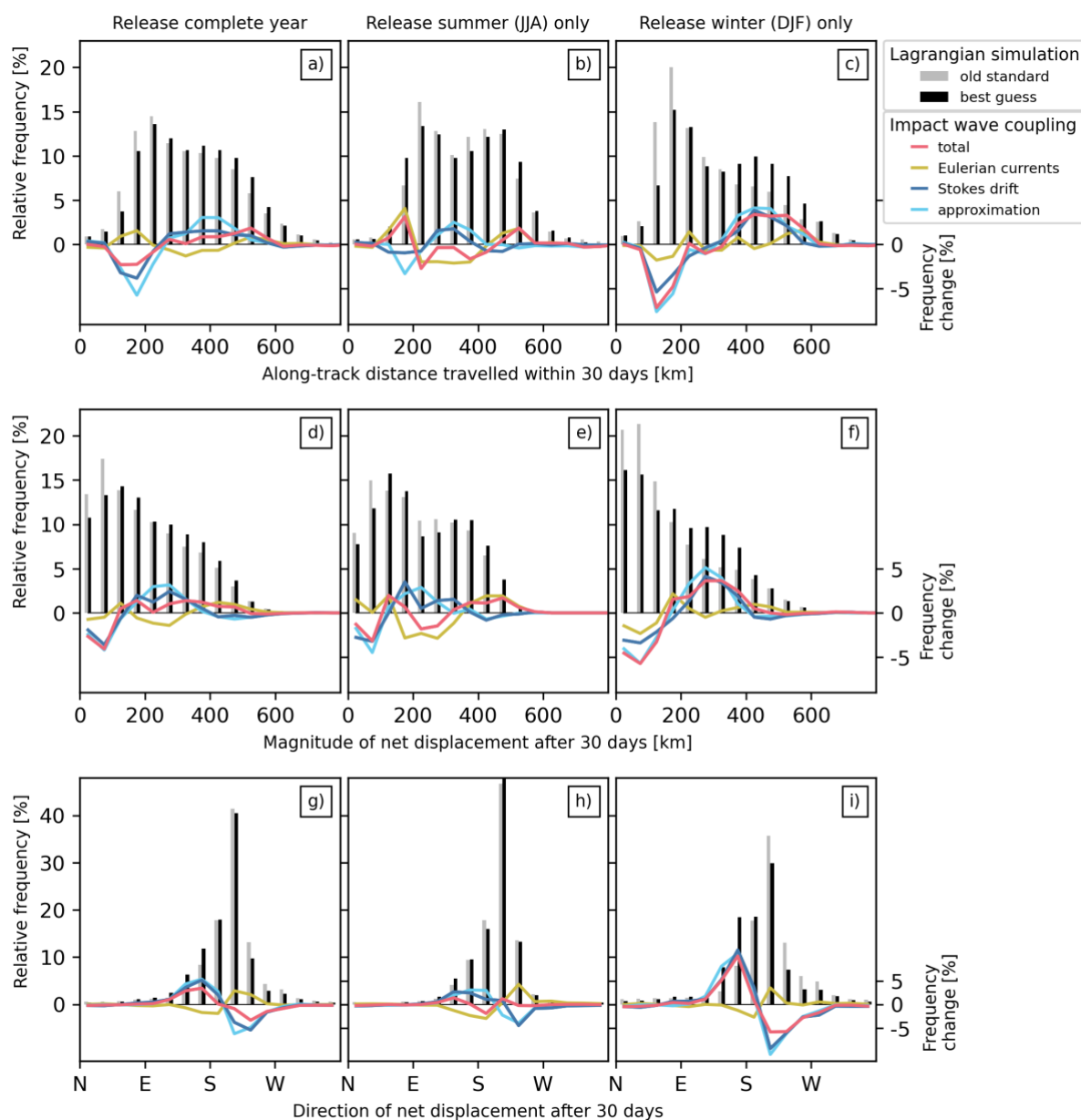
Figure 9: **Impact of surface waves on statistics of simulated dispersal of particles released in the Gulf of Lion (release 2, winter type region) at the end of the integration period of 30 days.** Shown are distributions of (a)-(c) the travelled along-track distance, as well as (d)-(f) the magnitude and (g)-(i) the direction of the net displacement for the old standard (grey bars) and best guess (black bars) simulations; the total change due to the wave coupling (red line), changes resulting from wave-driven Eulerian currents (yellow line) and Stokes drift (blue line) individually, as well as changes resulting from the basic approximation (cyan line) are overlaid.

The estimated connectivity to the Balearic Islands is similarly sensitive to the inclusion of wave-driven Eulerian currents: for summer, the inclusion of the impact of Stokes drift and wave-driven Eulerian currents together interrupts the connection between the Gulf of Lion and Mallorca, while connecting pathways still exist if only Stokes drift alone is added.

In summary, the results for this region support the hypothesis that applying the basic approximation in a winter type region generally leads to an improvement of the dispersal simulations. However, the analyses also reveal that applying the basic approximation is not sufficient to capture the total impact of waves on surface particle dispersal.

4.2.3 Gulf of Antalya in central-northern Levantine Sea (release 3, summer type region)

In the old standard simulation (Fig. 10a-c, grey bars in Fig. 11, Table 3), particles released in the Gulf of Antalya typically travel westward or south-eastward, reaching an average net displacement of 213 km after 30 days, while covering an average along-track distance of 417 km that translates into an average along-track speed of 0.16 ms^{-1}. As for the previously discussed regions, individual particle pathways vary significantly depending on the exact release location and time. Most notably, there are large differences between the summer and winter dispersal pattern. In summer, the south-eastward paths dominate, and the distance and displacement distributions show clear maxima around 400 km and 200 km, respectively, resulting in a well-defined area with the highest particle density just south of the release region. In winter, the westward pathways dominate, distance and displacement are on average higher but also show much broader distributions, resulting in a smaller retention rate, larger dispersal area, and less concentrated final particle distributions.

In the best guess simulation (Fig. 10d-f, black bars in Fig. 11, Table 3), the average along-track distance and displacements are reduced in summer (-10 % for both measures) but marginally increased in winter (+1 % for both measures) compared to the old standard simulation. This implies that the average along-track velocities are also decreased in summer but slightly increased in winter, though the Eulerian averages for the Lagrangian speed in the summer type region (Fig. 4) indicated a decrease for both seasons. This emphasizes that Lagrangian averages can deviate from Eulerian averages, since they depend on the exact trajectories of the particles, that is, on which part of the flow field they sample at what time and for how long. One would generally assume that Lagrangian means are smaller than Eulerian means, as particles spend more time in regions with slow background flow; however – as in the present case – Lagrangian averaging can also result in higher speeds, if particles are more confined to stronger currents. The dispersal area is decreased over the whole year (-2 % to -9 %), whereas the retention remains largely unchanged in summer but increases in winter (+23 %). Hence, for this region, there is no direct link between particle speed and dispersal area or retention rate, emphasizing again the importance of the exact pathways the particles take.

As expected for a summer type region, all net changes (red lines in Fig. 11) between the best guess and old standard simulations are dominated by changes in Eulerian currents (yellow lines in Fig. 11), Stokes drift (blue lines in Fig. 11) has a small net effect. Nevertheless, using the basic approximation (Fig. 10g-i, cyan line in Fig. 11), yields a small improvement over employing the old standard for several of the calculated dispersion measures (Table 3). This can be partly attributed to the fact that – in contrast to what has been discussed before – for these measures and in the considered region, the basic approximation

560 introduces net changes that act approximately in the same direction as the wave-driven Eulerian currents (which, however, partially differ from changes due to Stokes drift in the best guess simulation).

To conclude, our results do not support the hypothesis that applying the old standard instead of the basic approximation generally leads to an improvement of the dispersal simulations in the chosen summer type region; for some dispersal measures it does, while for others it does not.
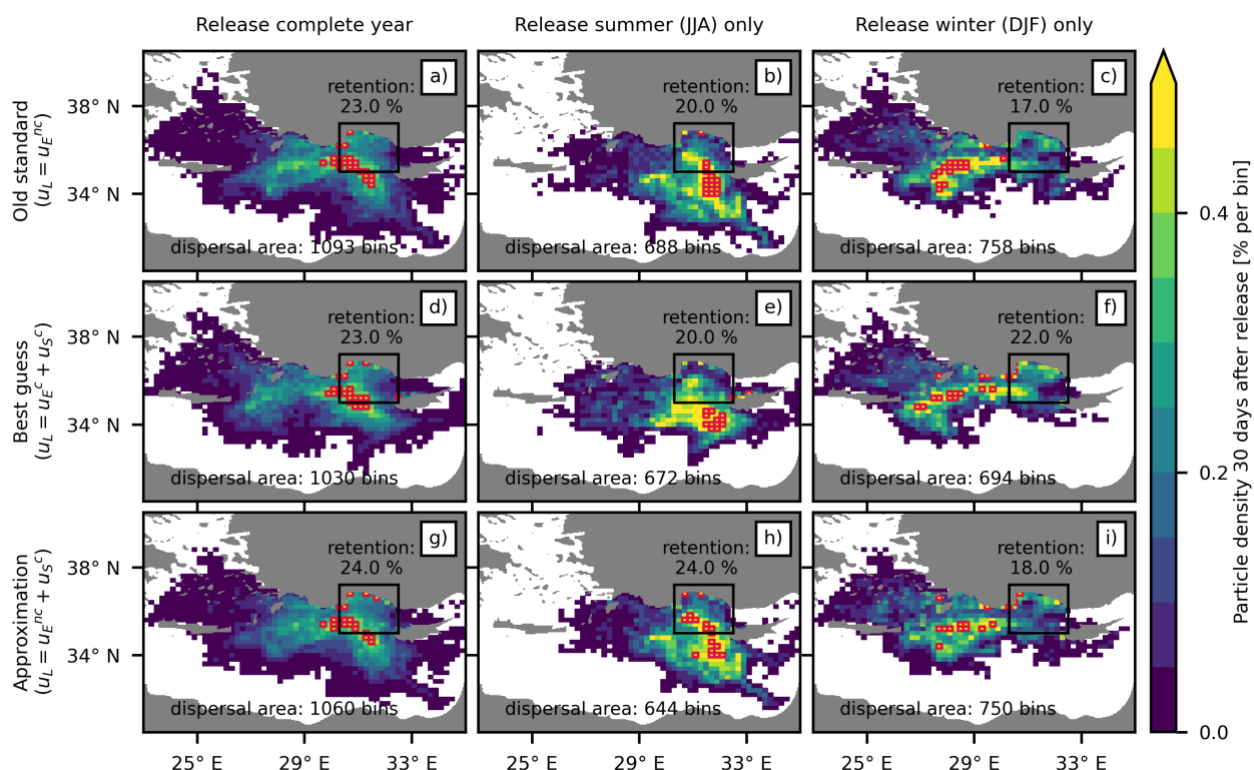
565

Figure 10: **Impact of surface waves on simulated dispersal pattern of particles released in the Gulf of Antalya (release 3, summer type region).** Shown is the particle density per 0.2° x 0.2° bin at the end of the integration period of 30 days (color shading); the area with the highest particle density, encompassing in total 10 % of the particle, is highlighted in red. For better comparability, values of the retention rate (percentage of particles that remain within or have returned to the region's release 570 area, indicated by the black frame, until the end of the integration period) and the overall dispersal area (total number of bins occupied with particles) are printed.

Figure 11: **Impact of surface waves on statistics of simulated dispersal of particles released in the Gulf of Antalya (release 3, summer type region) at the end of the integration period of 30 days**. Shown are distributions of (a)-(c) the travelled along-track distance, as well as (d)-(f) the magnitude and (g)-(i) the direction of the net displacement for the old standard (grey bars) and best guess (black bars) simulations; the total change due to the wave coupling (red line), changes resulting from wave-driven Eulerian currents (yellow line) and Stokes drift (blue line) individually, as well as changes resulting from the basic approximation (cyan line) are overlayed.

5 Summary and Discussion

580 We used the output of a newly developed coupled ocean-wave model configuration and complementary stand-alone ocean model configuration for the Mediterranean Sea to quantify how Stokes drift and wave-driven Eulerian currents impact simulated idealized surface particle dispersal. Moreover, we assessed how well this combined wave impact is represented in surface particle dispersal simulations that make use of the basic approximation, i.e., that employ a superposition of non-wave-driven Eulerian currents and Stokes drift obtained from independently run ocean and wave models for the particle tracking.

585 We find that Stokes drift as well as wave-driven Eulerian currents can have a non-negligible impact on surface particle dispersal. While both tend to act in opposing directions, they do not necessarily offset one another at the surface, due to different temporal and spatial variability. Our analyses suggest a seasonal and regional dependency of the wave impact. For most of the Mediterranean Sea, ocean-wave coupling increases the simulated mean Lagrangian surface speed in winter through a dominant impact of Stokes drift and decreases it in summer through a dominant impact by wave-driven Eulerian currents.

590 Yet, some regions also exhibit a dominant impact of either Stokes drift or wave-driven Eulerian currents throughout the whole year. Consequently, applying the commonly used basic approximation is not always beneficial for surface particle simulations. For summer and in regions where the impact of wave-driven Eulerian currents dominates for the whole year, as well as for time periods during which wave-driven Eulerian currents and Stokes drift effects tend to offset one another, it can be better to utilize the old standard approach for particle dispersal simulations, that is, ignoring any wave effect. In addition, we highlight

595 that the advantages and disadvantages of applying the basic approximation versus the old standard further depend on the Lagrangian measure of interest (cf., Table 3). One measure may be adequately represented by the basic approximation, another one by the old standard, and a third one by neither of the two simulation types that exclude wave-driven Eulerian currents. However, due to the complex interplay of wave-driven Eulerian currents, Stokes drift, and the regional non-wave-driven circulation, these dependencies cannot be known a priori. Hence, we argue that – whenever possible – coupled ocean-wave

600 models should be employed for surface particle dispersal simulations. This is especially true for studies that heavily rely on the accuracy of individual or low probability particle tracks, such as the estimation of connectivity patterns.

We acknowledge, however, that our results are based on idealized particle dispersal simulations for a short period utilizing one specific regional one-way coupled ocean-wave model configuration. More studies with output from other fully coupled ocean-wave models spanning larger regions and longer periods are needed to further investigate the spatial and temporal variability

605 of the impact of Stokes drift and wave-driven Eulerian currents not only on idealized but also on realistic particle dispersal simulations. Open questions to be addressed by these follow-up studies include: How robust is the different seasonality of the impact of Stokes drift and wave-driven Eulerian currents and what are its major drivers? What is the relative importance of the impact of Stokes drift and wave-driven Eulerian currents on much shorter (i.e. hourly) and longer (i.e. decadal) timescales? Which role does intrinsic variability play? Case-specific simulations for real applications with non-idealized particles can yield

610 additional insights on how important wave impacts are compared to other particle type specific factors such as windage or vertical motion. These analyses will indicate which findings from past studies relying on dispersal simulations without coupled

ocean-wave models should be revisited. They can also be used to further improve the accuracy of Lagrangian dispersal simulations for which coupled ocean-wave model output remains unavailable.

5.1 Comparison with previous studies

615 Our results complement the findings of, e.g., Röhrs et al. (2012) and Cunningham et al. (2022), that – while Stokes drift often represents the dominant impact of waves on surface particle dispersal – wave-driven Eulerian currents can significantly alter dispersal patterns and need to be considered to accurately represent the impact of waves on surface particle dispersal simulations.

Why do other studies lead to conflicting results and suggest that only the Stokes drift needs to be included (e.g., Tamtare et
620 al., 2022) or the wave impact does not need to be considered at all (e.g., Wagner et al., 2022)? This controversy can partially be related to methodological issues. We highlighted that Eulerian and Lagrangian averages may be significantly different, dependent on which regions of the flow are sampled by the Lagrangian trajectories at what time and for how long. Moreover, differences in spatio-temporal variability of non-coupled and coupled ocean-wave models may cancel out in a Eulerian mean sense but can accumulate along a Lagrangian trajectory; this effect can become even more pronounced with longer trajectory
625 integration times. We argue that analyzing Lagrangian velocities in an Eulerian framework is insufficient for estimating the impact of certain flow components such as Stokes drift and wave-driven Eulerian currents on large-scale particle dispersal patterns. Study-specific Lagrangian simulations are required to capture the whole impact. Following this argument, the analysis of Wagner et al. (2022) remains partially inconclusive and there is no evidence that surface velocities from ocean models without the inclusion of any surface wave impact indeed represent actual particle drift velocities.

630 Furthermore, the validation of simulated surface particle drift trajectories remains challenging. Available comparisons between simulated and observed drifter trajectories do not allow for a clear separation of the impact of Stokes drift and other wind-and wave-induced particle drift. As surface drifters are subject to direct wind drag, they are not only advected by ocean surface velocities but experience an additional drift in the wind direction. In particle simulations this is often accounted for via an additional leeway term $\alpha \boldsymbol{u}_A$, also referred to as the wind correction term:

635 $$\boldsymbol{u}_L = \boldsymbol{u}_E + \boldsymbol{u}_S + \alpha \boldsymbol{u}_A \qquad (10)$$

with $\boldsymbol{u}_A$ representing the near surface atmospheric wind speed and α a dimensionless parameter that is empirically determined to minimize differences between observed and simulated trajectories (e.g., Tamtare et al., 2022; Röhrs et al., 2012). Since Stokes drift approximately aligns with the wind direction and a substantial part of the wave-driven Eulerian currents tend to act in the opposing direction of Stokes drift, the tuning of α can to some degree also compensate for an under- or overestimation
640 of Stokes drift and negligence of wave-driven Eulerian currents in $\boldsymbol{u}_E$. Likewise, we argue – in contrast to Tamtare et al. (2022) – that an improved agreement between observed and simulated drifter trajectories when including only Eulerian currents and Stokes drift from independently run ocean and wave models and omitting the wind correction term does not necessarily imply that windage and other remaining drivers such as wave-driven currents are negligible. Those additional factors also could tend

to offset one another. Or, if velocity products including data assimilation are employed, part of their impact may even be
645   included in the Eulerian current fields. However, whether certain drift components partly or completely oppose each other
depends on the intricate interplay between regional ocean current dynamics, prevailing wind and wave patterns, and drifter
design. It is then a natural consequence that some specific Lagrangian drift models with inclusion of Stokes drift benefit from
a wind correction term (Tamtare et al., 2022; Callies et al., 2017) while others do not (e.g., De Dominicis et al., 2013; Lebreton
et al., 2018).

5.2 Potential implications for 3D particle dispersal simulations

While our analysis focused on 2D horizontal surface particle dispersal simulations, our results also have implications for 3D
particle dispersal simulations. We highlighted that Stokes drift and horizontal wave-driven Eulerian currents are both strongest
at the sea surface but show differences in their vertical profiles and temporal variability. The vertical Stokes drift profile can
be directly inferred from surface wave characteristics, e.g., as defined by Eq. (2), and the overall magnitude of the Stokes drift
655   exhibits a relatively clear seasonality with maximum values in winter. In contrast, the vertical profile of horizontal wave-driven
Eulerian currents is influenced by a range of processes that act on larger depth scales than Stokes drift and result in more
complex temporal variability. In general, horizontal wave-driven Eulerian currents tend to be less surface intensified during
periods with strong vertical mixing such as in fall and winter. Moreover, we find first indications of different sub-surface
regimes of the surface wave impact on Lagrangian velocities roughly corresponding to the Stokes layer, the Ekman layer, and
660   the deep ocean (cf. Fig. 2, not shown in detail). While impacts in the deep ocean most likely predominantly arise from a
reduced strength of the surface wind stress forcing (which is reducing overall oceanic current strengths), changes in the Stokes
layer are dominated by Stokes drift and anti-Stokes forces, and changes in the Ekman layer compose of effects from reduced
surface wind stress, anti-Stokes forces, and stratification changes due to wave-induced mixing. Consequently, to properly
resolve the impact of waves on 3D particle dispersal simulations, the different vertical profiles of Stokes drift and horizontal
665   wave-driven Eulerian currents need to be considered. Ideally, that also includes advanced formulations for the vertical Stokes
drift profile that better account for swell, as for example described in Breivik and Christensen (2020). Moreover, the impact
of surface waves on vertical particle velocities should be included in 3D Lagrangian dispersal simulations. This concerns
changes in the vertical velocities arising from horizontal divergence of the resolved flow as described in Eq. (7), as well as
turbulent vertical motions responsible for wave-induced increases in mixing such as Langmuir turbulence (cf. van Sebille et
670   al. (2020) and references therein).

5.3 Role of open-ocean Stokes drift for beaching

Finally, we would like to emphasize that – in contrast to what has been reported in various previous studies (Bosi et al., 2021;
Delandmeter and van Sebille, 2019) – no significant beaching of particles occurred in our simulations, independent of whether
Stokes drift was added. This can be attributed to the fact that all the employed velocity fields (Eulerian currents and Stokes

675 drift) are provided on the same grid with zero velocities from ocean to land and the particle tracking scheme respecting this boundary condition. While a detailed analysis of this matter is beyond the scope of this paper, it calls for a reassessment of how realistic simulated Lagrangian particle beaching statistics are, if they include – or even fully rely on – beaching introduced by open-ocean Stokes drift provided on a non-matching grid with non-zero velocities from ocean to land. We suggest that adding open-ocean Stokes drift to the Eulerian current velocities of a large-scale ocean model should not result in particles

680 leaving the ocean domain, but instead should only change the probability of particles reaching and staying in the last ocean grid cells next to the coast. The beaching or grounding itself – if relevant for the type of particle under consideration – can then be obtained from a Lagrangian parameterization that accounts for all known unresolved processes occurring at the sub-grid scale that are ultimately responsible for pushing particles ashore (Pawlowicz, 2021). There is an increasing number of, for example, marine plastic dispersal studies with basic implementations of this approach (Onink et al., 2019; Ypma et al.,

685 2022; Kaandorp et al., 2023; Vogt-Vincent et al., 2023; Liubartseva et al., 2018; van der Mheen et al., 2020). Yet, the existing grounding parameterizations still need further refinement and validation based on data from dedicated grounding experiments with customized surface drifters (Pawlowicz, 2021).

6 Conclusions

Returning to the two main research questions of our study, based on our idealized Lagrangian analyses with a newly developed

690 high-resolution (1/24°) coupled ocean-wave model configuration for the Mediterranean Sea, we draw the following conclusions:

(1) Stokes drift and wave-driven Eulerian currents can have a non-negligible impact on surface particle dispersal, often tend to act in opposing directions, but do not necessarily offset one another due to different temporal variability and spatial variations.

695 (2) If coupled ocean-wave model output is not available, the basic approximation of the wave impact via adding Stokes drift from a separately run wave model may not always be beneficial when compared to not including any wave impact. However, the error of including Stokes drift versus not including any wave impact varies temporally and spatially and depends on the Lagrangian dispersal measure of interest. The benefit or disadvantage of applying the basic approximation is difficult to obtain a priori.

700 More coupled ocean-wave model output – especially longer and global-scale – is needed to further quantify the time and space dependent relative impact of wave-driven Eulerian currents versus Stokes drift and to improve the accuracy of surface particle dispersal simulations.

Appendices

Appendix A: Calculation of Eulerian current and Stokes drift contributions to horizontal Lagrangian speed

705 For the coupled ocean-wave model, the Stokes drift and Eulerian current contributions to the horizontal Lagrangian speed $\|\boldsymbol{u}_L^c\|$ are obtained via the scalar projections of the Stokes drift velocity $\boldsymbol{u}_S^c$ and the horizontal Eulerian current velocity $\boldsymbol{u}_E^c$ onto the total horizontal Lagrangian velocity vector $\boldsymbol{u}_L^c$, denoted as $comp_{\boldsymbol{u}_L^c}\boldsymbol{u}_S^c$ and $comp_{\boldsymbol{u}_L^c}\boldsymbol{u}_E^c$ respectively (Figure A1):

$$comp_{\boldsymbol{u}_L^c}\boldsymbol{u}_S^c = \|\boldsymbol{u}_S^c\|\cos\alpha = \frac{\boldsymbol{u}_L^c \cdot \boldsymbol{u}_S^c}{\|\boldsymbol{u}_L^c\|}, \tag{11}$$

$$comp_{\boldsymbol{u}_L^c}\boldsymbol{u}_E^c = \|\boldsymbol{u}_E^c\|\cos\beta = \frac{\boldsymbol{u}_L^c \cdot \boldsymbol{u}_E^c}{\|\boldsymbol{u}_L^c\|}, \tag{12}$$

710 with α being the angle between $\boldsymbol{u}_S^c$ and $\boldsymbol{u}_L^c$, and β being the angle between $\boldsymbol{u}_E^c$ and $\boldsymbol{u}_L^c$. The scalar projection is positive if the angle is smaller than 90° and negative if the angle is larger than 90° (and smaller than 180°), corresponding to an increasing and decreasing contribution to $\|\boldsymbol{u}_L^c\|$, respectively.
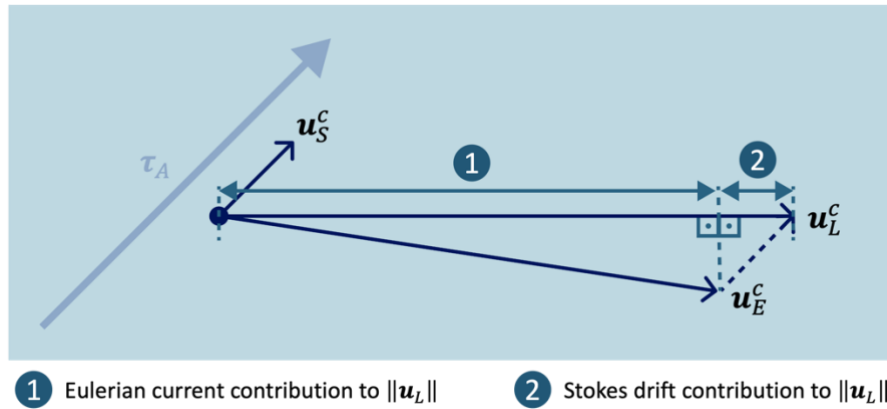
715 **Figure A1: Derivation of the Eulerian currents and Stokes drift contributions to the total horizontal Lagrangian speed $\|\boldsymbol{u}_L\|$ in the coupled ocean-wave model.** The Stokes drift and Eulerian current contributions to the horizontal Lagrangian speed $\|\boldsymbol{u}_L^c\|$ are obtained via the scalar projections of the Stokes drift velocity $\boldsymbol{u}_S^c$ and the horizontal Eulerian current velocity $\boldsymbol{u}_E^c$ onto the total horizontal Lagrangian velocity vector $\boldsymbol{u}_L^c$. The Stokes drift $\boldsymbol{u}_S^c$ is approximately aligned with the atmospheric wind stress $\boldsymbol{\tau}_A$, whereas $\boldsymbol{u}_L^c$ and $\boldsymbol{u}_E^c$ are deflected to the right of the wind (on the Northern Hemisphere).

720

Code and data availability

The surface velocities from the coupled and non-coupled model experiments employed in this study are publicly available on zenodo (https://zenodo.org/records/10879702; Moulin and Clementi, 2024a). The Lagrangian particle tracking code Parcels is available via https://github.com/OceanParcels/parcels or https://anaconda.org/conda-forge/parcels.

Author contributions

SR conceived the study, performed the Lagrangian simulations and all formal analyses, produced the figures, and wrote the manuscript. EC and AM developed the coupled-ocean wave model configuration, ran the hindcast experiments, and co-wrote the respective parts of the model description in Sect. 3. MCD contributed to the development of the employed Lagrangian analysis methods. TvdB contributed to the analysis of the effects of the wave-driven Eulerian currents. EvS secured the funding and supported the project conception and implementation within the framework of the IMMERSE project. All authors contributed to the final manuscript through critical review and editing.

Competing interests

Erik van Sebille is a member of the editorial board of Ocean Science.

Acknowledgements

SR and EvS were partly supported through the IMMERSE project from the European Union Horizon 2020 Research and Innovation Program (grant agreement no. 821926). The ocean-wave model simulations were performed using the CMCC high-performance computing infrastructure; the Lagrangian trajectory simulations and all other model analyses were conducted using the high-performance computing infrastructure at Utrecht University (Lorenz). We thank the IMMERSE and DRAKKAR communities for their continuous contributions to the development and validation of the employed model configurations, and the whole Lagrangian Oceanography team at Utrecht University for discussions on and technical support of our Lagrangian analyses methods.

References

Ardhuin, F., Rogers, E., Babanin, A. V., Filipot, J. F., Magne, R., Roland, A., van der Westhuysen, A., Queffeulou, P., Lefevre, J. M., Aouf, L., and Collard, F.: Semiempirical Dissipation Source Functions for Ocean Waves. Part I: Definition, Calibration, and Validation, J Phys Oceanogr, 40, 1917–1941, https://doi.org/10.1175/2010JPO4324.1, 2010.

Barbariol, F., Davison, S., Falcieri, F. M., Ferretti, R., Ricchi, A., Sclavo, M., and Benetazzo, A.: Wind Waves in the
Mediterranean Sea: An ERA5 Reanalysis Wind-Based Climatology, Front Mar Sci, 8, 760614,
https://doi.org/10.3389/FMARS.2021.760614/BIBTEX, 2021.

750 Battjes, J. A. and Janssen, J. P. F. M.: Energy loss and set-up due to breaking of random waves, Coastal Engineering
Proceedings, 1, 32, https://doi.org/10.9753/icce.v16.32, 1978.

Bosi, S., Broström, G., and Roquet, F.: The Role of Stokes Drift in the Dispersal of North Atlantic Surface Marine Debris,
Front Mar Sci, 8, 1137, https://doi.org/10.3389/FMARS.2021.697430/BIBTEX, 2021.

Breivik, Ø. and Christensen, K. H.: A Combined Stokes Drift Profile under Swell and Wind Sea, J Phys Oceanogr, 50,
755 2819–2833, https://doi.org/10.1175/JPO-D-20-0087.1, 2020.

Breivik, Ø., Allen, A. A., Maisondieu, C., and Olagnon, M.: Advances in search and rescue at sea Topical Collection on
Advances in Search and Rescue at Sea, Ocean Dyn, 63, 83–88, https://doi.org/10.1007/S10236-012-0581-1/METRICS,
2013.

Breivik, Ø., Mogensen, K., Bidlot, J. R., Balmaseda, M. A., and Janssen, P. A. E. M.: Surface wave effects in the NEMO
760 ocean model: Forced and coupled experiments, J Geophys Res Oceans, 120, 2973–2992,
https://doi.org/10.1002/2014JC010565, 2015.

Breivik, Ø., Bidlot, J.-R., and Janssen, P. A. E. M.: A Stokes drift approximation based on the Phillips spectrum, Ocean
Model (Oxf), 100, 49–56, https://doi.org/10.1016/j.ocemod.2016.01.005, 2016.

van den Bremer, T. S. and Breivik: Stokes drift, Philosophical Transactions of the Royal Society A: Mathematical, Physical
765 and Engineering Sciences, 376, https://doi.org/10.1098/RSTA.2017.0104, 2018.

Bressan, A. and Constantin, A.: The Deflection Angle of Surface Ocean Currents From the Wind Direction, J Geophys Res
Oceans, 124, 7412–7420, https://doi.org/10.1029/2019JC015454, 2019.

Callies, U., Groll, N., Horstmann, J., Kapitza, H., Klein, H., Maßmann, S., and Schwichtenberg, F.: Surface drifters in the
German Bight: Model validation considering windage and Stokes drift, Ocean Science, 13, 799–827,
770 https://doi.org/10.5194/OS-13-799-2017, 2017.

Charnock, H.: Wind stress on a water surface, Quarterly Journal of the Royal Meteorological Society, 81, 639–640,
https://doi.org/10.1002/QJ.49708135027, 1955.

Christensen, A., Mariani, P., and Payne, M. R.: A generic framework for individual-based modelling and physical-biological
interaction, PLoS One, 13, e0189956, https://doi.org/10.1371/JOURNAL.PONE.0189956, 2018.

775 Clarke, A. J. and van Gorder, S.: The Relationship of Near-Surface Flow, Stokes Drift and the Wind Stress, J Geophys Res
Oceans, 123, 4680–4692, https://doi.org/10.1029/2018JC014102, 2018.

Clementi, E., Oddo, P., Drudi, M., Pinardi, N., Korres, G., and Grandi, A.: Coupling hydrodynamic and wave models: first
step and sensitivity experiments in the Mediterranean Sea, Ocean Dyn, 67, 1293–1312, https://doi.org/10.1007/s10236-
017-1087-7, 2017.

780 Clementi, E. , Aydogdu, A., Goglio, A., Pistoia, J., Escudier, R., Drudi, M., Grandi, A., Mariani, A., Lyubartsev, V., Lecci, R., Cretí, S., Coppini, G., Masina, S., and Pinardi, N.: Mediterranean Sea Physical Analysis and Forecast (CMEMS MED-Currents, EAS6 system) (Version 1) [Data set], https://doi.org/10.25423/CMCC/MEDSEA_ANALYSISFORECAST_PHY_006_013_EAS6, 2021.

Couvelard, X., Lemarié, F., Samson, G., Redelsperger, J. L., Ardhuin, F., Benshila, R., and Madec, G.: Development of a
785 two-way-coupled ocean-wave model: Assessment on a global NEMO(v3.6)-WW3(v6.02) coupled configuration, Geosci Model Dev, 13, 3067–3090, https://doi.org/10.5194/GMD-13-3067-2020, 2020.

Craig, A., Valcke, S., and Coquart, L.: Development and performance of a new version of the OASIS coupler, OASIS3-MCT-3.0, Geosci Model Dev, 10, 3297–3308, https://doi.org/10.5194/GMD-10-3297-2017, 2017.

Craig, P. D. and Banner, M. L.: Modeling Wave-Enhanced Turbulence in the Ocean Surface Layer, J Phys Oceanogr, 24,
790 2546–2559, https://doi.org/10.1175/1520-0485(1994)024<2546:MWETIT>2.0.CO;2, 1994.

Craik, A. D. D. and Leibovich, S.: A rational model for Langmuir circulations, J Fluid Mech, 73, 401–426, https://doi.org/10.1017/S0022112076001420, 1976.

Cunningham, H. J., Higgins, C., and van den Bremer, T. S.: The Role of the Unsteady Surface Wave-Driven Ekman–Stokes Flow in the Accumulation of Floating Marine Litter, J Geophys Res Oceans, 127, e2021JC018106,
795 https://doi.org/10.1029/2021JC018106, 2022.

Delandmeter, P. and van Sebille, E.: The Parcels v2.0 Lagrangian framework: New field interpolation schemes, Geosci Model Dev, 12, 3571–3584, https://doi.org/10.5194/gmd-12-3571-2019, 2019.

De Dominicis, M., Pinardi, N., Zodiatis, G., and Lardner, R.: MEDSLIK-II, a Lagrangian marine surface oil spill model for short-term forecasting-Part 1: Theory, Geosci Model Dev, 6, 1851–1869, https://doi.org/10.5194/gmd-6-1851-2013,
800 2013.

Drennan, W. M., Kahma, K. K., Terray, E. A., Donelan, M. A., and Kitaigorodskii, S. A.: Observations of the Enhancement of Kinetic Energy Dissipation Beneath Breaking Wind Waves, Breaking Waves, 95–101, https://doi.org/10.1007/978-3-642-84847-6_6, 1992.

Guha, A. and Gupta, A.: Understanding Stokes drift mechanism via crest and trough phase estimates, arXiv (preprint),
805 https://doi.org/10.48550/arXiv.2303.07464, 2023.

Hasselmann, K.: Wave-driven inertial oscillations, Geophysical and Astrophysical Fluid Dynamics, 1, 463–502, https://doi.org/10.1080/03091927009365783, 1970.

Hasselmann, K.: On the mass and momentum transfer between short gravity waves and larger-scale motions, J Fluid Mech, 50, 189–205, https://doi.org/10.1017/S0022112071002520, 1971.

810 Hasselmann, S. and Hasselmann, K.: Computations and Parameterizations of the Nonlinear Energy Transfer in a Gravity-Wave Spectrum. Part I: A New Method for Efficient Computations of the Exact Nonlinear Transfer Integral, J Phys Oceanogr, 15, 1369–1377, https://doi.org/10.1175/1520-0485(1985)015<1369:CAPOTN>2.0.CO;2, 1985.

Hellerman, S. and Rosenstein, M.: Normal Monthly Wind Stress Over the World Ocean with Error Estimates, J Phys Oceanogr, 13, 1093–1104, https://doi.org/10.1175/1520-0485(1983)013<1093:NMWSOT>2.0.CO;2, 1983.

815 Higgins, C., Vanneste, J., and van den Bremer, T. S.: Unsteady Ekman-Stokes Dynamics: Implications for Surface Wave-Induced Drift of Floating Marine Litter, Geophys Res Lett, 47, https://doi.org/10.1029/2020GL089189, 2020.

Janssen, P., Breivik, Ø., Mogensen, K., Vitart, F., Balmaseda, M., Bidlot, J.-R., Keeley, S., Leutbecher, M., Magnusson, L., and Molteni, F.: Air-Sea Interaction and Surface Waves, ECMWF Technical Memorandum 712, 2013.

Kaandorp, M. L. A., Lobelle, D., Kehl, C., Dijkstra, H. A., and van Sebille, E.: Global mass of buoyant marine plastics
820 dominated by large long-lived debris, Nature Geoscience 2023 16:8, 16, 689–694, https://doi.org/10.1038/s41561-023-01216-0, 2023.

Lange, M. and van Sebille, E.: Parcels v0.9: prototyping a Lagrangian ocean analysis framework for the petascale age, Geosci Model Dev, 10, 4175–4186, https://doi.org/10.5194/gmd-10-4175-2017, 2017.

Large, G. and Yeager, S.: Diurnal to decadal global forcing for ocean and sea-ice models: The data sets and flux
825 climatologies, https://doi.org/10.5065/D6KK98Q6, 2004.

Lebreton, L., Slat, B., Ferrari, F., Sainte-Rose, B., Aitken, J., Marthouse, R., Hajbane, S., Cunsolo, S., Schwarz, A., Levivier, A., Noble, K., Debeljak, P., Maral, H., Schoeneich-Argent, R., Brambini, R., and Reisser, J.: Evidence that the Great Pacific Garbage Patch is rapidly accumulating plastic, Scientific Reports 2018 8:1, 8, 1–15, https://doi.org/10.1038/s41598-018-22939-w, 2018.

830 Lewis, D. M. and Belcher, S. E.: Time-dependent, coupled, Ekman boundary layer solutions incorporating Stokes drift, Dynamics of Atmospheres and Oceans, 37, 313–351, https://doi.org/10.1016/J.DYNATMOCE.2003.11.001, 2004.

Li, S., Zou, Z., Zhao, D., and Hou, Y.: On the Wave State Dependence of the Sea Surface Roughness at Moderate Wind Speeds under Mixed Wave Conditions, J Phys Oceanogr, 50, 3295–3307, https://doi.org/10.1175/JPO-D-20-0102.1, 2020.

835 Liubartseva, S., Coppini, G., Lecci, R., and Clementi, E.: Tracking plastics in the Mediterranean: 2D Lagrangian model, Mar Pollut Bull, 129, 151–162, https://doi.org/10.1016/J.MARPOLBUL.2018.02.019, 2018.

Madec, G. and NEMO System team: NEMO ocean engine, Scientific Notes of Climate Modelling Center, 27 — ISSN 1288-1619, Institut Pierre-Simon Laplace (IPSL), https://doi.org/10.5281/ZENODO.6334656, 2022.

McWilliams, J. C. and Restrepo, J. M.: The Wave-Driven Ocean Circulation, J Phys Oceanogr, 29, 2523–2540,
840 https://doi.org/10.1175/1520-0485(1999)029<2523:TWDOC>2.0.CO;2, 1999.

van der Mheen, M., van Sebille, E., and Pattiaratchi, C.: Beaching patterns of plastic debris along the Indian Ocean rim, Ocean Science, 16, 1317–1336, https://doi.org/10.5194/OS-16-1317-2020, 2020.

Moulin, A. and Clementi, E.: Mediterranean Sea, NEMO4.2 / WW3 uncoupled and coupled surface: stress, currents and Stokes Drift [Data set], https://doi.org/10.5281/ZENODO.10879702, 2024a.

845   Moulin, A. and Clementi, E.: Mediterranean Sea, NEMO4.2/WW3 wave-current interactions, https://doi.org/10.25424/cmcc-qa6z-6t39, 2024b.

Onink, V., Wichmann, D., Delandmeter, P., and van Sebille, E.: The Role of Ekman Currents, Geostrophy, and Stokes Drift in the Accumulation of Floating Microplastic, J Geophys Res Oceans, 124, 1474–1490, https://doi.org/10.1029/2018JC014547, 2019.

850   Pawlowicz, R.: The Grounding of Floating Objects in a Marginal Sea, J Phys Oceanogr, 51, 537–551, https://doi.org/10.1175/JPO-D-20-0183.1, 2021.

Pettenuzzo, D., Large, W. G., and Pinardi, N.: On the corrections of ERA-40 surface flux products consistent with the Mediterranean heat and water budgets and the connection between basin surface total heat flux and NAO, J Geophys Res Oceans, 115, 6022, https://doi.org/10.1029/2009JC005631, 2010.

855   Rascle, N. and Ardhuin, F.: Drift and mixing under the ocean surface revisited: Stratified conditions and model-data comparisons, J Geophys Res Oceans, 114, 2016, https://doi.org/10.1029/2007JC004466, 2009.

Rascle, N., Ardhuin, F., and Terray, E. A.: Drift and mixing under the ocean surface: A coherent one-dimensional description with application to unstratified conditions, J Geophys Res Oceans, 111, 3016, https://doi.org/10.1029/2005JC003004, 2006.

860   Röhrs, J., Christensen, K. H., Hole, L. R., Broström, G., Drivdal, M., and Sundby, S.: Observation-based evaluation of surface wave effects on currents and trajectory forecasts, Ocean Dyn, 62, 1519–1533, https://doi.org/10.1007/S10236-012-0576-Y, 2012.

van Sebille, E., Griffies, S. M., Abernathey, R., Adams, T. P., Berlof, P., Biastoc, A., Blanke, B., Chassignet, E. P., Cheng, Y., Cotter, C. J., Deleersnijder, E., Döös, K., Drake, H., Drijfhout, S., Gar, S. F., Heemink, A. W., Kjellsson, J.,
865   Koszalka, I. M., Lange, M., Lique, C., MacGilchrist, G. A., Marsh, R., Adame, G. C. M., McAdam, R., Nencioli, F., Paris, C. B., Piggott, M. D., Polton, J. A., Rühs, S., Shah, S. H. A. M., Thomas, M. D., Wang, J., Wolfram, P. J., Zanna, L., and Zika, J. D.: Lagrangian ocean analysis: Fundamentals and practices, Ocean Model (Oxf), 121, 49–75, https://doi.org/10.1016/j.ocemod.2017.11.008, 2018.

van Sebille, E., Aliani, S., Law, K. L., Maximenko, N., Alsina, J. M., Bagaev, A., Bergmann, M., Chapron, B., Chubarenko,
870   I., Cózar, A., Delandmeter, P., Egger, M., Fox-Kemper, B., Garaba, S. P., Goddijn-Murphy, L., Hardesty, B. D., Hoffman, M. J., Isobe, A., Jongedijk, C. E., Kaandorp, M. L. A., Khatmullina, L., Koelmans, A. A., Kukulka, T., Laufkötter, C., Lebreton, L., Lobelle, D., Maes, C., Martinez-Vicente, V., Morales Maqueda, M. A., Poulain-Zarcos, M., Rodríguez, E., Ryan, P. G., Shanks, A. L., Shim, W. J., Suaria, G., Thiel, M., Van Den Bremer, T. S., and Wichmann, D.: The physical oceanography of the transport of floating marine debris, Environmental Research Letters, 15, 023003,
875   https://doi.org/10.1088/1748-9326/AB6D7D, 2020.

van Sebille, E., Zettler, E., Wienders, N., Amaral-Zettler, L., Elipot, S., and Lumpkin, R.: Dispersion of Surface Drifters in the Tropical Atlantic, Front Mar Sci, 7, 607426, https://doi.org/10.3389/FMARS.2020.607426, 2021.

Song, J. B.: The effects of random surface waves on the steady Ekman current solutions, Deep Sea Research Part I: Oceanographic Research Papers, 56, 659–671, https://doi.org/10.1016/J.DSR.2008.12.014, 2009.

880   Spaulding, M. L.: State of the art review and future directions in oil spill modeling, Mar Pollut Bull, 115, 7–19, https://doi.org/10.1016/J.MARPOLBUL.2017.01.001, 2017.

Stokes, G. G.: On the theory of oscillatory waves, Trans. Cam. Philos. Soc., 8, 441–455, 1847.

Sutherland, B. R., Dibenedetto, M., Kaminski, A., and Van Den Bremer, T.: Fluid dynamics challenges in predicting plastic pollution transport in the ocean: A perspective, Phys Rev Fluids, 8, 70701,

885   https://doi.org/10.1103/PhysRevFluids.8.070701, 2023.

Suzuki, N. and Fox-Kemper, B.: Understanding Stokes forces in the wave-averaged equations, J Geophys Res Oceans, 121, 3579–3596, https://doi.org/10.1002/2015JC011566, 2016.

Swearer, S. E., Treml, E. A., and Shima, J. S.: A review of biophysical models of marine larval dispersal, Oceanography and Marine Biology, 57, 325–356, https://doi.org/10.1201/9780429026379-7, 2019.

890   Tamtare, T., Dumont, D., and Chavanne, C.: The Stokes drift in ocean surface drift prediction, Journal of Operational Oceanography, 15, 156–168, https://doi.org/10.1080/1755876X.2021.1872229, 2022.

The WAVEWATCH III R© Development Group (WW3DG): User manual and system documentation of WAVEWATCH III R© version 6.07. Tech. Note 33, College Park, MD, USA, 465 pp. + Appendices, 2019.

Tolman, H. L.: Alleviating the Garden Sprinkler Effect in wind wave models, Ocean Model (Oxf), 4, 269–289,

895   https://doi.org/10.1016/S1463-5003(02)00004-5, 2002.

Tonani, M., Balmaseda, M., Bertino, L., Blockley, E., Brassington, G., Davidson, F., Drillet, Y., Hogan, P., Kuragano, T., Lee, T., Mehra, A., Paranathara, F., Tanajura, C. A. S., and Wang, H.: Status and future of global and regional ocean prediction systems, Journal of Operational Oceanography, 8, s201–s220, https://doi.org/10.1080/1755876X.2015.1049892, 2015.

900   Vogt-Vincent, N. S., Burt, A. J., Kaplan, D. M., Mitarai, S., Turnbull, L. A., and Johnson, H. L.: Sources of marine debris for Seychelles and other remote islands in the western Indian Ocean, Mar Pollut Bull, 187, 114497, https://doi.org/10.1016/J.MARPOLBUL.2022.114497, 2023.

Wagner, G. L., Constantinou, N. C., and Reichl, B. G.: Stokes drift should not be added to ocean general circulation model velocities, arXiv (preprint), https://doi.org/10.48550/arXiv.2210.08552, 2022.

905   Ypma, S. L., Bohte, Q., Forryan, A., Naveira Garabato, A. C., Donnelly, A., and van Sebille, E.: Detecting the most effective cleanup locations using network theory to reduce marine plastic debris: A case study in the Galapagos Marine Reserve, Ocean Science, 18, 1477–1490, https://doi.org/10.5194/os-18-1477-2022, 2022.